Conditional Mean First Passage Times to Small Traps in a 3-D Domain with a Sticky Boundary: Applications to T Cell Searching Behaviour in Lymph Nodes

M. I. DELGADO, M. J. WARD, D. COOMBS

Monica Delgado, Michael J. Ward, and Daniel Coombs; Department of Mathematics and Institute of Applied Mathematics, University of British Columbia, Vancouver, British Columbia, V6T 1Z2, Canada. (corresponding author: Daniel Coombs (coombs@math.ubc.ca))

(*Received 4 June 2015*)

Calculating the time required for a diffusing object to reach a small target within a larger domain is a feature of a large class of modeling and simulation efforts in biology. Here, we are motivated by the motion of a T cell of the immune system seeking a particular antigen-presenting-cell within a large lymph node. The precise nature of the cell motion at the outer boundary of the lymph node is not completely understood in terms of how cells choose to remain within a given lymph node, or exit. In previous work, we and others have studied diffusive motion to a small trap. We extend this previous work to analyze models where the diffusing object may exit the outer boundary of the domain (in this case, the lymph node). This is modeled by a Robin boundary condition on the surface of the lymph node. For the general problem of small traps inside a 3-D domain that has a partially sticky or absorbent domain boundary, the method of matched asymptotic expansions is used to calculate the mean and variance of the conditional first passage time for the T cell to reach a specific target trap. Our results are illustrated explicitly for the idealized situation of a spherical lymph node containing small spherically-shaped traps, and are verified for a radially symmetric geometry with one trap at the origin where exact solutions are available. Mathematically, our analysis extends previous work on the calculation of the MFPT by allowing for a sticky boundary and by calculating conditional statistics of the diffusion process. Finally, our results are interpreted and applied to the context of T cell biology.

Key words: Matched asymptotic expansions, small traps, splitting probability, conditional MFPT, sticky boundary.

1 Introduction

We analyze the time it takes for a randomly diffusing particle to reach a target region within a larger three-dimensional domain. In particular, we will study the mean and variance of the time to first contact in particular geometric configurations, including the case where the target region is very small compared to the overall domain. We are inspired by a typical search scenario from cellular immunology, where a T cell must search for a particular cell within a lymph node.

T cells play a very important role in the adaptive immune response. T cells originate in the bone marrow but then migrate to the thymus to undergo maturation. Mature T cells migrate to the peripheral lymphoid organs, which include lymph nodes. These are organized tissues where immune responses are initiated and where lymphocytes are maintained. The T cells then continually recirculate through these tissues.

During an infection, molecular signatures of pathogens are carried from the site of infection to the lymphoid organs by specialized cells called antigen presenting cells. Antigen (defined as any substance that can be recognized by the adaptive immune system) is "presented" by these cells as molecules bound to specialized cell surface receptors. T cells carry complementary surface receptors that can bind to particular antigens and this molecular interaction can then lead to T cell proliferation and differentiation into effector cells that are ready to fight the pathogens (for instance, by activating B cells to produce antibodies, or by directly killing infected cells). Therefore, in order for a particular T cell to become activated, it must come into contact with an antigen-presenting cell that is carrying the antigen molecules that it

recognizes. But especially during the earliest stages of infection, or in the cases of slow-growing infections, or infections with agents that can interfere with the process of antigen presentation, we can imagine that the antigen-presenting cells are rare. Therefore, the question of how long it takes for a particular T cell to find its antigen is clearly relevant to understanding the timing of the immune response. A more complete description of the biological situation is given in [**33**].

Lymph nodes are roughly ellipsoidal (sometimes partly concave in a kidney-bean shape) and are on the order of millimetres in size. They have a highly organized architecture where different parts of the organ appear to have different functions and contain different proportions of the different classes of immune cells [**33**]. We shall focus on a single T cell zone of a lymph node, where T cells are known to interact with antigen-presenting-cells and begin the response to foreign antigen (Figure. 1). We will model this as a spherical domain within which a single T cell seeks one or more antigen-presenting-cells that are small on the scale of the whole domain. The approximation of a spherical domain allows us to generate explicit formulae but is not important for the big picture of our approach.

Within the lymph node the motion of T cells has been established, via two-photon microscopy [**11**], to be consistent with an underlying random walk behavior when reasonably long time scales (greater than a few minutes) are considered [**32**, **50**, **12**, **31**]. However, it has also been experimentally established that T cells preferentially attach to, and move on, the fibroblastic reticular network (an array of filamentous cell structures that fill the relevant parts of the lymph node) [**2**, **39**]. For these reasons, theoretical and computational studies of T cell motion have generally been of two kinds: considering free movement in three-dimensional space [**51**, **5**, **25**, **47**, **13**, **46**, **20**] or emphasizing the importance of lattice-based motion [**34**, **4**, **3**, **9**, **23**, **22**, **24**, **48**]. Many of these previous approaches depend on extensive computation with fairly complex cellular-automaton models, requiring much detailed parameter estimation.

Here, we adopt an approach based on first-passage times for a mobile T cell to reach one of a number of fixed antigen-presenting cells located within a spherical lymph node (Fig. 1) We will model the T cell as a point particle undergoing Brownian motion, and the antigen-presenting cell as a small target within the larger lymph node. We will calculate the mean and variance for the time it takes the T cell to reach one of the targets in this idealized situation. We will consider two different stylized behaviors of the T cell at the boundary of the lymph node: (i) when the cell is unable to pass through the boundary; (ii) when the cell has a finite probability of passing through the boundary (and then never returns to the lymph node in this model). In this latter situation the boundary is said to be sticky or partially absorbent. Mathematically, these conditions correspond to either a reflecting (Neumann) or partially absorbing (Robin) boundary condition on the domain boundary. We will also consider the possible effects of other antigen-presenting cells within the domain, which act as barriers to T cell motion.

Our model of the lymph node can be critiqued on the grounds that T cells are not true random walkers, but rather demonstrate persistent motion, and spatially dependent effects that are evident in tracking data. We defend our approach against this criticism on the grounds of (i) simplicity; (ii) we have very few parameters to estimate; and (iii) many random walk processes appear diffusive when viewed on long time- or space-scales. Indeed, as shown in [**22**], a network-based model of T cell motion reduces to Brownian motion over medium- to long- time scales. Therefore, our work should be regarded as large-scale estimates, averaging over much of the cell-scale details. At the conclusion of this paper, we describe some possible extensions that add more realism to our model, and that warrant further investigation.

In our general theoretical framework, the lymph node is modeled by a bounded 3-D domain Ω with boundary $\partial\Omega$. The target antigen-presenting cell, Ω_{ε_1}, is taken to be an absorbing subdomain, or trap, of small radius of $\mathcal{O}(\varepsilon)$ centered at some point $\mathbf{x}_1 \in \Omega$. We will consider the presence of $M-1$ additional, non-overlapping subdomains or traps Ω_{ε_j} for $j = 2, \ldots, M$, each of small radius, corresponding to other antigen-presenting cells. These subdomains are centered at $\mathbf{x}_j$

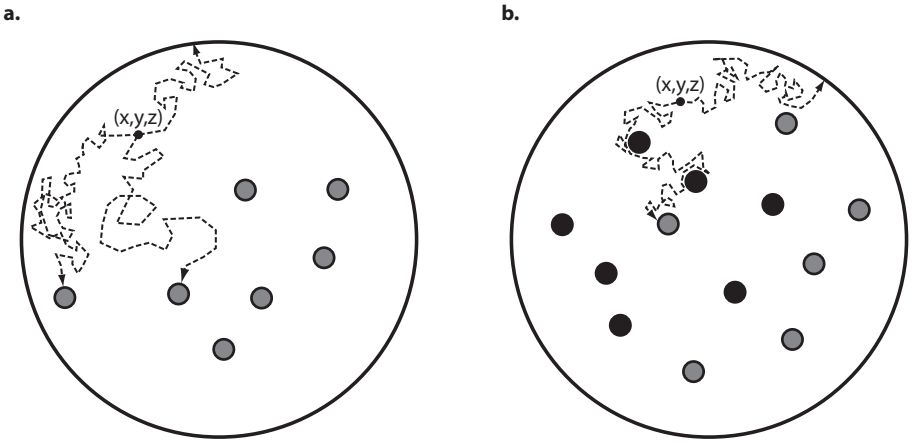

Figure 1. Schematic drawing of our model for T cell search. **a.** A single T cell (point particle) starts at (x, y, z) and then executes a random walk within a large spherical domain representing a stylized piece of lymphoid tissue. Upon reaching a relevant antigen-presenting-cell (any of the grey patches), the T cell's search is completed. Alternatively, the T cell might reach the boundary first. We consider different cases for the cell behaviour at the boundary: reflection (followed by continued search); absorption (corresponding to exiting the lymph node) and partially absorbing (where there is a fixed probability of immediately exiting the spherical domain). **b.** We also consider the situation where there are irrelevant antigen-presenting-cells (black patches) that act as passive barriers to motion.

for $j = 2, \ldots, M$. The diffusing searcher (the T cell) has diffusion constant D and begins its search somewhere in $\Omega \backslash \Omega_p$, where $\Omega_p \equiv \cup_{i=1}^{M} \Omega_{\varepsilon_j}$. The asymptotic limit that we will consider is where the diameter of each absorber is asymptotically smaller than the diameter of Ω. Primarily, we will focus our analysis on the distinguished limit where the probability of reaching the target trap is of the same asymptotic order in ε of becoming absorbed by the partially sticky domain boundary. A partially absorbing (Robin) boundary condition can be thought of as a homogeneous alternative to small absorbing traps on the boundary (studied in [**41**]) or the use of "killing sites" for diffusion in a narrow geometry [**26**]. We do not take these possibilities any further in this paper.

Since the searcher is not always guaranteed to find the target, we define the *Splitting Probability* $\mathcal{P}(\mathbf{x})$ to be the probability that a searcher starting at $\mathbf{x}$ reaches the target before being absorbed by either the sticky boundary or the other traps. We then define the moments of the first passage time distribution, conditional on the searcher reaching the target, as follows: $\mathbb{T}$ is the mean first passage time (MFPT), and the N-th moment is written as $\mathbb{T}_{\mathbb{N}}$. The concepts of first passage time and splitting probability for diffusive processes are described completely in the books of Redner [**35**] and (in more detail), in Karlin and Taylor [**29**].

From a purely theoretical viewpoint, our work here is an extension of the results in [**17**], [**15**], [**45**], and [**36**] on the mean first passage time (MFPT) for capture of a diffusing particle by a trap in a 3-D domain. In [**17**], the matched asymptotic expansion methodology of [**49**], which was developed to treat problems having strong localized perturbations, was extended to derive a 2-term expansion for the splitting probability and for the MFPT for the capture of a Brownian particle at any one of a collection of small traps. For a collection of small spherical traps, a 3-term expansion for the splitting probability and the MFPT was obtained in [**15**] using a pseudo-potential type approach. These results were carefully reviewed in the context of T cell motion in [**21**]. With the exception of the work in [**45**] and [**36**] for a specific 2-D and 3-D domain, respectively, we are not aware of any previous analysis determining conditional statistics, such as the conditional MFPT and variance, for narrow capture problems in arbitrary 3-D domains with a collection of small traps.

In this paper, we first extend the analysis of [**17**] to calculate the splitting probability and MFPT for a Robin boundary condition, which models a partially sticky or absorbent outer boundary. Under this Robin condition, we also calculate the conditional MFPT and conditional variance to a specific trap in an arbitrary 3-D domain. The results are then illustrated explicitly for a spherical domain containing a finite collection of small traps.

In §2, we review and extend previous work to provide PDE's for the MFPT, the splitting probability, and the higher moments. Explicit calculations for a spherically symmetric geometry that has exactly one absorbing target centered at the origin are given. In §3 we asymptotically calculate the splitting probability for the general situation of a 3-D domain with sticky boundary that contains one target trap and additional non-target traps. In §4 we asymptotically calculate the conditional mean first passage time MFPT and the conditional second moment for this problem. In this way, we obtain an asymptotic formula for the conditional variance for the time required to reach the target. For the special case where Ω is a sphere containing small spherically-shaped traps, explicit analytical results are obtained in §3 and §4 for the splitting probability, and the conditional MFPT and variance. In §5 we consider the related problem of calculating the MFPT, the second moment, and the variance of the time needed for a diffusing particle to become absorbed at either any one of a collection of traps in a 3-D domain or on the sticky boundary. Our results for this problem are an extension of those of [**17**] where the MFPT was calculated for the case of a perfectly reflecting boundary. Finally, in §6, we apply our results to T cell biology where realistic parameter values are selected and we describe some related open problems.

The problems under consideration in this paper can be collectively referred to as *narrow capture problems*, where the time needed for a Brownian particle to reach a small compact target in a 3-D domain is asymptotically long as the radius of the target tends to zero. More broadly, a detailed survey of the analysis of diffusive and directed motion of proteins towards small target binding sites in mathematical models of intracellular transport is given in [**7**] and [**10**]. A mathematically related class of problems, known as *narrow escape problems*, where a Brownian particle can exit a domain only through a small window on its boundary, have been studied by formal asymptotics in [**42**] and [**16**], and rigorously by potential-theoretic methods in [**14**]. A related narrow escape problem involving multiple switching gates was studied in [**1**]. A broad survey of narrow escape problems and their applications to biophysical modeling, together with rather comprehensive reference lists, is given in [**27**] and [**40**].

2 Splitting Probability and First-Passage Time Distributions

2.1 Reflecting Boundary Conditions

The simplest situation is where Ω contains one trap Ω_a and where there is a reflecting (Neumann) boundary condition imposed at the boundary $\partial\Omega$. In this case, the splitting probability $\mathcal{P}$ is $\mathcal{P} \equiv 1$, and it is well known [**35**, **37**] that the MFPT satisfies the Poisson equation

$$\triangle \mathbb{T} = -\frac{1}{D}\,, \quad \mathbf{x} \in \Omega\backslash\Omega_a\,; \qquad \mathbb{T} = 0\,, \quad \mathbf{x} \in \partial\Omega_a\,; \qquad \partial_n \mathbb{T} = 0\,, \quad \mathbf{x} \in \partial\Omega\,, \tag{2.1}$$

where ∂_n denotes the outward normal derivative. There is also a hierarchy of equations for $N \geq 2$ defining the higher moments, where we have labeled $\mathbb{T}_1 \equiv \mathbb{T}$, given by

$$\triangle \mathbb{T}_N = -\frac{N\mathbb{T}_{N-1}}{D}\,, \quad \mathbf{x} \in \Omega\backslash\Omega_a\,; \qquad \mathbb{T}_N = 0\,, \quad \mathbf{x} \in \partial\Omega_a\,; \qquad \partial_n \mathbb{T}_N = 0\,, \quad \mathbf{x} \in \partial\Omega\,. \tag{2.2}$$

In the special case where Ω is a sphere of radius L containing a concentric target sphere Ω_a of radius a centered at the origin, then from (2.1) we readily obtain the MFPT for a particle starting at distance r from the origin given by

$$\mathbb{T}(r) = \frac{(r-a)}{3D}\left(\frac{L^3}{ar} - \frac{a+r}{2}\right)\,. \tag{2.3 a}$$

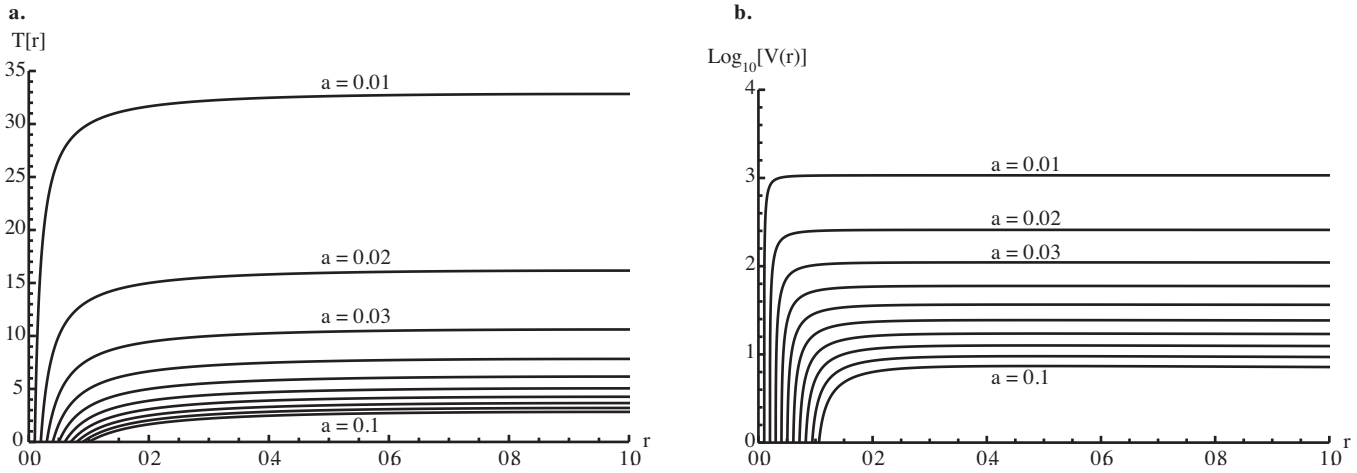

Figure 2. Mean and variance for spherically symmetric one-trap model with Neumann boundary conditions. Space and time are rescaled so that the domain radius L and the diffusion coefficient D are eliminated from the expressions for $\mathbb{T}$ and $\mathbb{V}$. **a.** The mean first passage time $\mathbb{T}(r)$ is plotted for a range of trap radii $a = 0.01, 0.02, \ldots, 0.09, 0.1$. **b.** The log of the variance of the first passage time $\mathbb{V}(r)$ is plotted for the same trap radii.

By re-scaling space and introducing $\epsilon = a/L$, $x = r/L$, we can write (2.3 *a*) in terms of ε as

$$\mathbb{T}(x) = \frac{L^2}{3D}\left(\frac{1}{\epsilon} - \frac{x^3+2}{2x} + \frac{1}{2}\epsilon^2\right). \tag{2.3 b}$$

The second moment $\mathbb{T}_2$ can also be obtained directly, leading to expressions for the variance of the first passage time, which we denote by $\mathbb{V}$, in dimensional (r) and rescaled (x) coordinates:

$$\mathbb{V}(r) = \mathbb{T}_2 - \mathbb{T}^2 = \frac{1}{D^2}\left(\frac{L^6}{9}\left(\frac{1}{a^2} - \frac{1}{r^2}\right) - \frac{2L^5}{5}\left(\frac{1}{a} - \frac{1}{r}\right) + \frac{2L^3}{9}(a-r) + \frac{(a^4 - r^4)}{90}\right), \tag{2.4 a}$$

$$\mathbb{V}(x) = \frac{L^4}{D^2}\left(\frac{1}{9\epsilon^2} - \frac{2}{5\epsilon} - \left(\frac{x^6 + 20x^3 - 36x + 10}{90x^2}\right) + \frac{2\epsilon}{9} + \frac{\epsilon^4}{90}\right). \tag{2.4 b}$$

This shows that $\mathbb{T} = \mathcal{O}(\varepsilon^{-1})$ and $\mathbb{V} = \mathcal{O}(\varepsilon^{-2})$. This mean and variance are plotted in Fig. 2.

2.2 Perfectly- and Partially- Absorbing Boundary Conditions

In the case of perfectly absorbing (Dirichlet) or partially absorbing (Robin) conditions on $\partial\Omega$, it is possible that a particle starting at x can exit the domain and so never reach the target site. Therefore, the splitting probability $\mathcal{P}(x)$ must be calculated along with the conditional moments of the first passage time. A derivation of the relevant PDEs and boundary conditions for the splitting probability and MFPT is given by Redner [**35**] for the case of perfectly absorbing boundaries. However, we were not able to find the equations for the higher moments with partially absorbing boundary conditions in the literature. Fortunately, the derivations are not difficult, following the same general procedure as in Redner (see sections 1.6.3 and 3.5.2 of [**35**]). We summarize these results below.

To obtain $\mathcal{P}(x)$, we sum the individual probabilities for all paths that start at x and reach the absorbing target, i.e.

$$\mathcal{P}(x) = \sum_{p \in paths} P_p(x), \tag{2.5}$$

where P_p is the probability of the path p. Now the sum over all possible paths can be decomposed into the outcome after one step and the sum over all path remainders from the intermediate point x'. We follow Redner [**35**] by discretizing space and time and working in one dimension only. The extension to higher spatial dimensions is completely straightforward.

We suppose that in a time step δt the particle will take a step of size δx either left or right, with equal probability, so that

$$\mathcal{P}(x) = \sum_p \left[\frac{1}{2}P_p(x+\delta x) + \frac{1}{2}P_p(x-\delta x)\right] = \frac{1}{2}\left[\mathcal{P}(x+\delta x) + \mathcal{P}(x-\delta x)\right]. \tag{2.6}$$

Upon writing the Taylor expansions of $\mathcal{P}(x \pm \delta x)$ and taking the limit $\delta x \to 0$ we obtain that $\mathcal{P}$ satisfies

$$\Delta\mathcal{P}(x) = 0, \qquad x \in \Omega\backslash\Omega_a. \tag{2.7}$$

Now we consider the behavior of the particle at the boundary. We apply a simplified version of the jump process description of Collins and Kimball for the behaviour of a Brownian particle in the vicinity of a partially-absorbing boundary [**19**]. Suppose that if the particle reaches a (partially) absorbing boundary at $x = L$ then it either takes a step of size δx back into the domain with probability $1 - \lambda(\delta x)$, or is absorbed with probability $\lambda(\delta x)$. In other words, the probability of getting to $L - \delta x$ from L in a time step of size δt, i.e. $p(L - \delta x, \delta t|L)$, is $1 - \lambda(\delta x)$. Assume also that the probability function λ satisfies $\lambda(\delta x) = \lambda_0 \delta x$, where λ_0 is a constant. Therefore, we have

$$\mathcal{P}(L) = (1-\lambda)\mathcal{P}(L-\delta x) \approx (1-\lambda)\left[\mathcal{P}(L) - \delta x\mathcal{P}'(L)\right], \tag{2.8}$$

where we have used a Taylor approximation. This yields that

$$(1-\lambda)\delta x\mathcal{P}'(L) = -\lambda\mathcal{P}(L).$$

Dividing by δx and letting $\delta x \to 0$ we obtain the following Robin condition for $\mathcal{P}$ on the boundary at $x = L$:

$$\mathcal{P}'(L) = -\lambda_0\mathcal{P}(L). \tag{2.9}$$

Note that when $\lambda_0 = 0$, this boundary condition corresponds to the perfectly reflecting boundary [**35**] while when $\lambda_0 \to \infty$, we find $\mathcal{P}(L) \to 0$, correctly corresponding to a perfectly absorbing boundary.

We now derive the equations for the MFPT and higher moments by a similar procedure. By their definitions, the MFPT $\mathbb{T} \equiv \mathbb{T}_1$ and higher moments $\mathbb{T}_N$ can be written as

$$\mathbb{T}_N(x) = \frac{\sum_{p\in paths} P_p(x)\, t_p^N(x)}{\sum_{p\in paths} P_p(x)}, \qquad \text{for } N = 1, 2, \ldots, \tag{2.10}$$

where $t_p(x)$ represents the time it takes for the particle to go from x to the target following path p. Multiplying through and considering a single (discretized) step of the (one-dimensional) process, we obtain

$$\mathcal{P}(x)\mathbb{T}_N(x) = \sum_p \left[\frac{1}{2}P_p(x+\delta x)\left(t_p(x+\delta x)+\delta t\right)^N + \frac{1}{2}P_p(x-\delta x)\left(t_p(x-\delta x)+\delta t\right)^N\right].$$

After expanding the powers of N and retaining terms up to $O(\delta t)$ we find

$$\mathcal{P}(x)\mathbb{T}_N(x) = \frac{1}{2}\sum_p \left[P_p(x+\delta x)\left(t_p(x+\delta x)^N + Nt_p(x+\delta x)^{N-1}\delta t\right) + P_p(x-\delta x)\left(t_p(x-\delta x)^N + Nt_p(x-\delta x)^{N-1}\delta t\right)\right].$$

It is now possible to rewrite the sums using equation (2.10) to obtain

$$\begin{aligned}\mathcal{P}(x)\mathbb{T}_N(x) = \frac{1}{2}&\left[\mathcal{P}(x+\delta x)\mathbb{T}_N(x+\delta x) + \mathcal{P}(x-\delta x)\mathbb{T}_N(x-\delta x)\right] \\ &+\delta t\frac{N}{2}\left[\mathcal{P}(x+\delta x)\mathbb{T}_{N-1}(x+\delta x) + \mathcal{P}(x-\delta x)\mathbb{T}_{N-1}(x-\delta x)\right].\end{aligned}$$

The last step is to Taylor expand in δx and retain terms up to $O(\delta x^2)$. After rearranging terms, this yields

$$0 = \frac{\delta x^2}{2\delta t}\Delta\left[\mathcal{P}(x)\mathbb{T}_N(x)\right] + N\mathcal{P}(x)\mathbb{T}_{N-1}(x).$$

Now taking the diffusion limit with $D = \delta x^2/(2\delta t)$ fixed, we obtain the general PDE for the moments in the case of Robin or Dirichlet boundaries, given by $\Delta\left[\mathcal{P}(x)\mathbb{T}_N(x)\right] = -N\mathcal{P}(x)\mathbb{T}_{N-1}(x)$.

We continue this derivation to determine the boundary conditions at a boundary point L. From (2.10) and our Robin boundary assumption we have

$$\begin{aligned}\mathcal{P}(L)\mathbb{T}_N(L) &= \sum_p (1-\lambda)\, P_p\,(L-\delta x)\,(t_p\,(L-\delta x)+\delta t)^N\ ,\\ &= \delta t\,(1-\lambda)\,\mathcal{P}\,(L-\delta x) + (1-\lambda)\,\mathcal{P}\,(L-\delta x)\,\mathbb{T}_N\,(L-\delta x)\ ,\\ &= \delta t\mathcal{P}\,(L) + (1-\lambda)\left[\mathcal{P}(L)\mathbb{T}_N(L) - \delta x\left[\mathcal{P}\mathbb{T}_N\right]'(L)\right]\ ,\end{aligned}$$

where we have used (2.8) and made a Taylor approximation of $\mathcal{P}\mathbb{T}$ about L to obtain the last line. This yields

$$(1-\lambda)\,\delta x\left[\mathcal{P}\mathbb{T}_N\right]'(L) = \delta t\mathcal{P}\,(L) - \lambda\mathcal{P}(L)\mathbb{T}_N(L)\,.$$

Upon taking the diffusion limit and using $\lambda\,(\delta x)\to\lambda_0\delta x$ we get

$$(1-\lambda_0\delta x)\left[\mathcal{P}\mathbb{T}\right]'(L) = \frac{\delta x}{2D}\mathcal{P}\,(L) - \lambda_0\left[\mathcal{P}\mathbb{T}\right](L)\ .$$

Again taking the limit as $\delta x\to 0$ gives the desired partially absorbing boundary condition,

$$\left[\mathcal{P}\mathbb{T}_N\right]'(L) = -\lambda_0\mathcal{P}(L)\mathbb{T}_N(L)\,. \tag{2.11}$$

In this way, we obtain the following system characterizing the MFPT to an absorbing target located concentrically within a partially absorbing spherical boundary of radius L, conditional on reaching the target at $\partial\Omega$:

$$D\Delta\left[\mathcal{P}\mathbb{T}\right](x) = -\mathcal{P}\,(x)\quad x\in\Omega\backslash\Omega_a\,;\qquad \left[\mathcal{P}\mathbb{T}\right]'(L) = -\lambda_0\mathcal{P}(L)\mathbb{T}(L)\,;\quad \left[\mathcal{P}\mathbb{T}\right](x) = 0\,,\quad x\in\partial\Omega_a\,, \tag{2.12}$$

where the splitting probability $\mathcal{P}$ satisfies

$$D\Delta\mathcal{P}\,(x) = 0\qquad x\in\Omega\backslash\Omega_a\,;\qquad \left[\mathcal{P}\right]'(L) = -\lambda_0\mathcal{P}(L)\,;\qquad \mathcal{P}\,(x) = 0\qquad x\in\partial\Omega_a\,. \tag{2.13}$$

Ignoring any interior traps (so $\mathcal{P}=1$), this Robin condition might be viewed as a homogenized limit of the effect of a large collection of isolated traps on the sphere boundary. This idea was discussed in approximate terms by Berg and Purcell in their classic paper, albeit in the context of diffusion to the exterior of a spherical cell [**8**]. The relevant limit for the case we consider here was examined in great detail in a recent paper of Cheviakov and Zawada [**18**].

For the special case of a perfectly absorbing outer boundary where $\lambda_0\to\infty$, then (2.12) and (2.13) reduce to the well-known system in Redner [**35**]. The PDE characterizing the higher moments is

$$\begin{aligned}D\Delta\left[\mathcal{P}\mathbb{T}_N\right](x) &= -N\mathcal{P}\,(x)\,\mathbb{T}_{N-1}(x)\qquad x\in\Omega\backslash\Omega_a\,,\\ \left[\mathcal{P}\mathbb{T}_N\right]'(L) &= -\lambda_0\mathcal{P}(L)\mathbb{T}_N(L)\,;\qquad \left[\mathcal{P}\mathbb{T}_N\right](x) = 0\qquad x\in\partial\Omega_a\,.\end{aligned} \tag{2.14}$$

Below in §3–5, we will replace λ_0 with λ in (2.12), (2.13), and (2.14), for notational simplicity.

2.3 A Radially Symmetric Geometry

We consider the special case of an absorbing target of radius a centered within a larger sphere of radius L, but now with a partially absorbing boundary on the larger sphere. For this case, we solve (2.13) and (2.12) to obtain

$$\mathcal{P}\,(r) = \frac{a\left(\lambda L^2-\lambda Lr+r\right)}{r\left(\lambda L^2-\lambda La+a\right)} = 1-\frac{\lambda L^2(r-a)}{\lambda rL(L-a)+ar}\,, \tag{2.15 a}$$

$$\mathbb{T}(r) = \frac{1}{6D}\left[(r-a)(2L-r-a)+2L\left(\frac{(L-a)^2}{a(1-\lambda L)+\lambda L^2}-\frac{(L-r)^2}{r(1-\lambda L)+\lambda L^2}\right)\right]\,. \tag{2.15 b}$$

It is also possible to use a computer algebra system such as Mathematica or Maple to calculate the second moment and then the variance of the first passage time. However, the expressions are rather unwieldy in the general case. In the limit $\lambda \to \infty$, corresponding to perfectly absorbing boundary conditions, we can calculate $\mathcal{P}$, $\mathbb{T}$ and the variance $\mathbb{V}$, as

$$\mathcal{P}(r) = \frac{a(r-L)}{r(a-L)} = \frac{\epsilon(x-1)}{x(\epsilon-1)} = \left(\frac{1}{x}-1\right)\left(\epsilon+\epsilon^2+\epsilon^3+\dots\right) \tag{2.16 a}$$

$$\mathbb{T}(r) = \frac{(r-a)(2L-r-a)}{6D} = \frac{L^2}{6D}\left(x(2-x)-2\epsilon+\epsilon^2\right) \tag{2.16 b}$$

$$\mathbb{V}(r) = \frac{\left((a-r)^2-(r-L)^2\right)\left((a-L)^2+(r-L)^2\right)}{90D^2}\,, \tag{2.16 c}$$

where again we have set $\epsilon = a/L$ and $x = r/L$. Similarly, by taking the limit $\lambda \to 0$, we can regain the expressions for the Neumann boundary case given in (2.3) and (2.4) above. Figures 3 and 4 show the splitting probability and the mean and variance of the conditional first passage times for the problem with Dirichlet and Robin boundary conditions, respectively.

Having established the relevant systems of PDE's defining the splitting probability and first passage time moments, in the next three sections we consider the general problem of how long it takes for a T cell to find its antigen specific APC, when it is surrounded by other non-specific APCs. We will examine the following problems: (i) the probability of contacting a particular target before any others, and (ii) the MFPT to reach a particular target conditional on reaching the target site. For each problem, we analyze the effect of different boundary conditions, corresponding to different T cell behaviours at the edge of the lymph node.

3 Splitting Probability with a Sticky Boundary

The splitting probability $\mathcal{P}(\mathbf{x})$ is the probability of reaching a specific target trap Ω_{ε_1} from an initial source point $\mathbf{x}$, before reaching either the sticky domain boundary or any of the other traps Ω_{ε_j} for $j = 2, \dots, M$. It satisfies

$$\Delta\mathcal{P} = 0\,, \quad \mathbf{x} \in \Omega\backslash\Omega_p \equiv \cup_{j=1}^{M}\Omega_{\varepsilon_j}\,; \qquad \partial_n\mathcal{P} + \lambda\mathcal{P} = 0\,, \quad \mathbf{x} \in \partial\Omega\,, \tag{3.1 a}$$

$$\mathcal{P} = 1\,, \quad \mathbf{x} \in \partial\Omega_{\epsilon_1}\,; \qquad \mathcal{P} = 0\,, \quad \mathbf{x} \in \partial\Omega_{\epsilon_j}\,, \quad j = 2, \dots, M\,. \tag{3.1 b}$$

Here Ω_{ε_j} for $j = 1, \dots, M$ are small subdomains of Ω of radii $\mathcal{O}(\varepsilon) \ll 1$ for which $\Omega_{\varepsilon_j} \to \mathbf{x}_j$ as $\varepsilon \to 0$.

We will first consider the distinguished scaling regime $\lambda = \mathcal{O}(\varepsilon)$, for which the boundary is only slightly sticky. As such, we define a boundary trapping parameter $\kappa > 0$ with $\kappa = \mathcal{O}(1)$ by

$$\lambda = \varepsilon\kappa\,. \tag{3.2}$$

We now solve (3.1) asymptotically as $\varepsilon \to 0$ by using the method of matched asymptotic expansions. In the outer region, defined away from the traps, we expand $\mathcal{P}$ as

$$\mathcal{P} = \mathcal{P}_0 + \varepsilon\mathcal{P}_1 + \varepsilon^2\mathcal{P}_2 + \cdots\,. \tag{3.3}$$

Here $\mathcal{P}_0$ is an unknown constant, and from (3.1 a) we obtain that $\mathcal{P}_k$ for $k = 1, 2$ satisfies

$$\Delta\mathcal{P}_k = 0\,, \qquad \mathbf{x} \in \Omega\backslash\{\mathbf{x}_1, \dots, \mathbf{x}_M\}\,; \qquad \partial_n\mathcal{P}_k = -\kappa\mathcal{P}_{k-1}\,, \qquad \mathbf{x} \in \partial\Omega\,, \tag{3.4}$$

with certain singularity conditions as $\mathbf{x} \to \mathbf{x}_j$ for $j = 1, \dots, M$ that are determined upon matching to the inner solution.

In the inner region near the j-th trap, we expand the inner solution $w(\mathbf{y}_j) \equiv \mathcal{P}(\mathbf{x}_j + \varepsilon\mathbf{y}_j)$, with $\mathbf{y}_j \equiv \varepsilon^{-1}(\mathbf{x} - \mathbf{x}_j)$, as

$$w = w_0 + \varepsilon w_1 + \cdots\,. \tag{3.5}$$

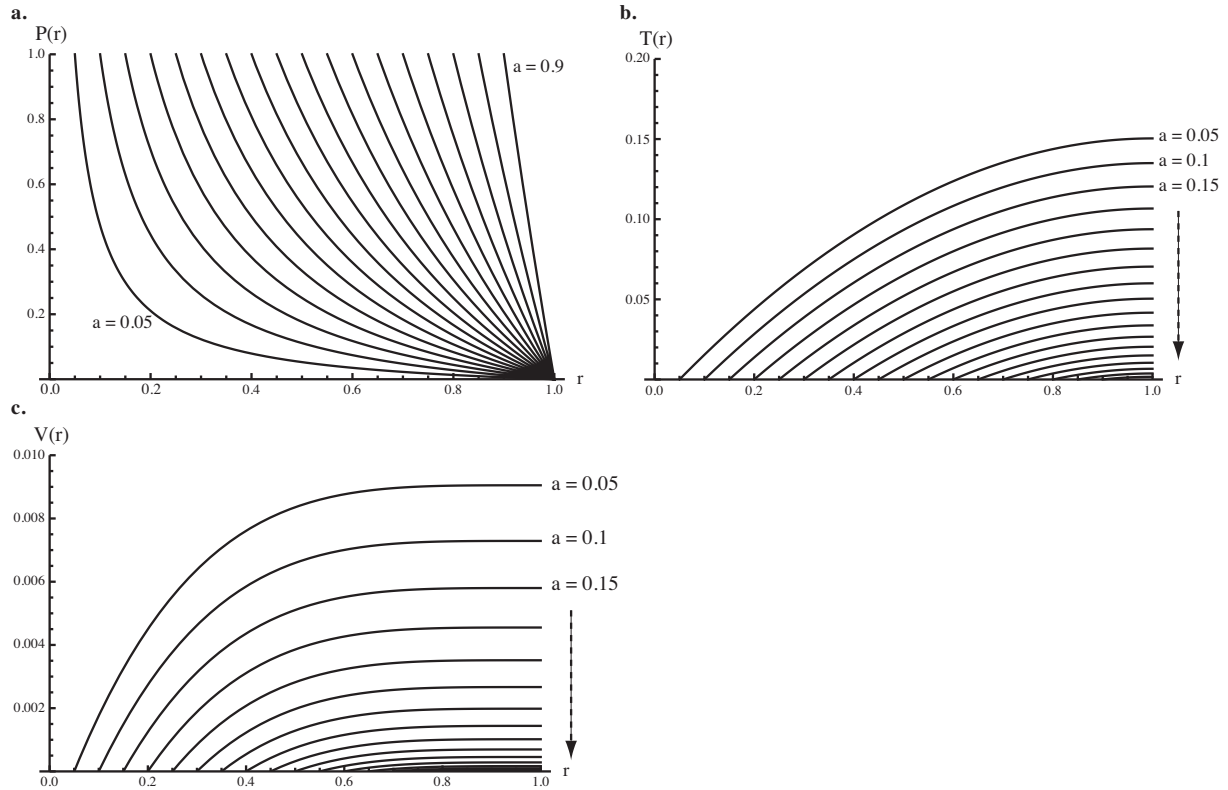

Figure 3. Splitting probability, mean and variance for spherically symmetric one-trap model with Dirichlet boundary conditions. Space and time are rescaled so that the domain radius L and the diffusion coefficient D are eliminated from all expressions. **a.** The probability of reaching the target $\mathbb{P}(r)$ is plotted for a range of trap radii $a = 0.05, 0.10, \ldots, 0.85, 0.90$. **b.** The conditional mean first passage time to the target, $\mathbb{T}(r)$, is plotted for the same range of trap radii. **c.** Variance of the first passage time $\mathbb{V}(r)$ is plotted for the same trap radii.

Upon substituting (3.5) into (3.1 *b*) and the PDE of (3.1 *a*), we obtain that w_0 and w_1 satisfy

$$\Delta_y w_0 = 0\,, \quad \mathbf{y}_j \notin \Omega_j\,; \qquad w_0 = \delta_{j1}\,, \quad \mathbf{y}_j \in \partial\Omega_j\,, \tag{3.6 a}$$

$$\Delta_y w_1 = 0\,, \quad \mathbf{y}_j \notin \Omega_j\,; \qquad w_1 = 0\,, \quad \mathbf{y}_j \in \partial\Omega_j\,. \tag{3.6 b}$$

Here $\Omega_j \equiv \varepsilon^{-1}\Omega_{\varepsilon_j}$, and δ_{j1} is Kronecker's symbol. The far-field boundary conditions for w_0 and w_1 are determined by the matching condition as $\mathbf{x} \to \mathbf{x}_j$ between the the inner and outer expansions (3.5) and (3.3), respectively, written as

$$\mathcal{P}_0 + \varepsilon\mathcal{P}_1 + \varepsilon^2\mathcal{P}_2 + \cdots \sim w_0 + \varepsilon w_1 + \cdots\,. \tag{3.7}$$

The first matching condition is that $w_0 \sim \mathcal{P}_0$ as $|\mathbf{y}_j| \to \infty$, where $\mathcal{P}_0$ is an unknown constant. Then, the solution for w_0 in the j-th inner region is given by

$$w_0 = \mathcal{P}_0 + (\delta_{j1} - \mathcal{P}_0)\, w_{cj}(\mathbf{y}_j)\,, \tag{3.8}$$

where w_{cj} is the solution to the classical capacitance problem in electrostatics given by

$$\Delta_y w_{cj} = 0\,, \quad \mathbf{y}_j \notin \Omega_j\,; \qquad w_{cj} = 1\,, \quad \mathbf{y}_j \in \partial\Omega_j\,; \qquad w_{cj} \to 0 \quad \text{as} \quad |\mathbf{y}_j| \to \infty\,. \tag{3.9 a}$$

It is well-known that the far-field behavior of w_c is (cf. [**28**])

$$w_{cj} \sim \frac{c_j}{|\mathbf{y}_j|} + \frac{\mathbf{b}_j\cdot\mathbf{y}_j}{|\mathbf{y}_j|^3} + \cdots \qquad \text{as} \quad |\mathbf{y}_j| \to \infty\,, \tag{3.9 b}$$

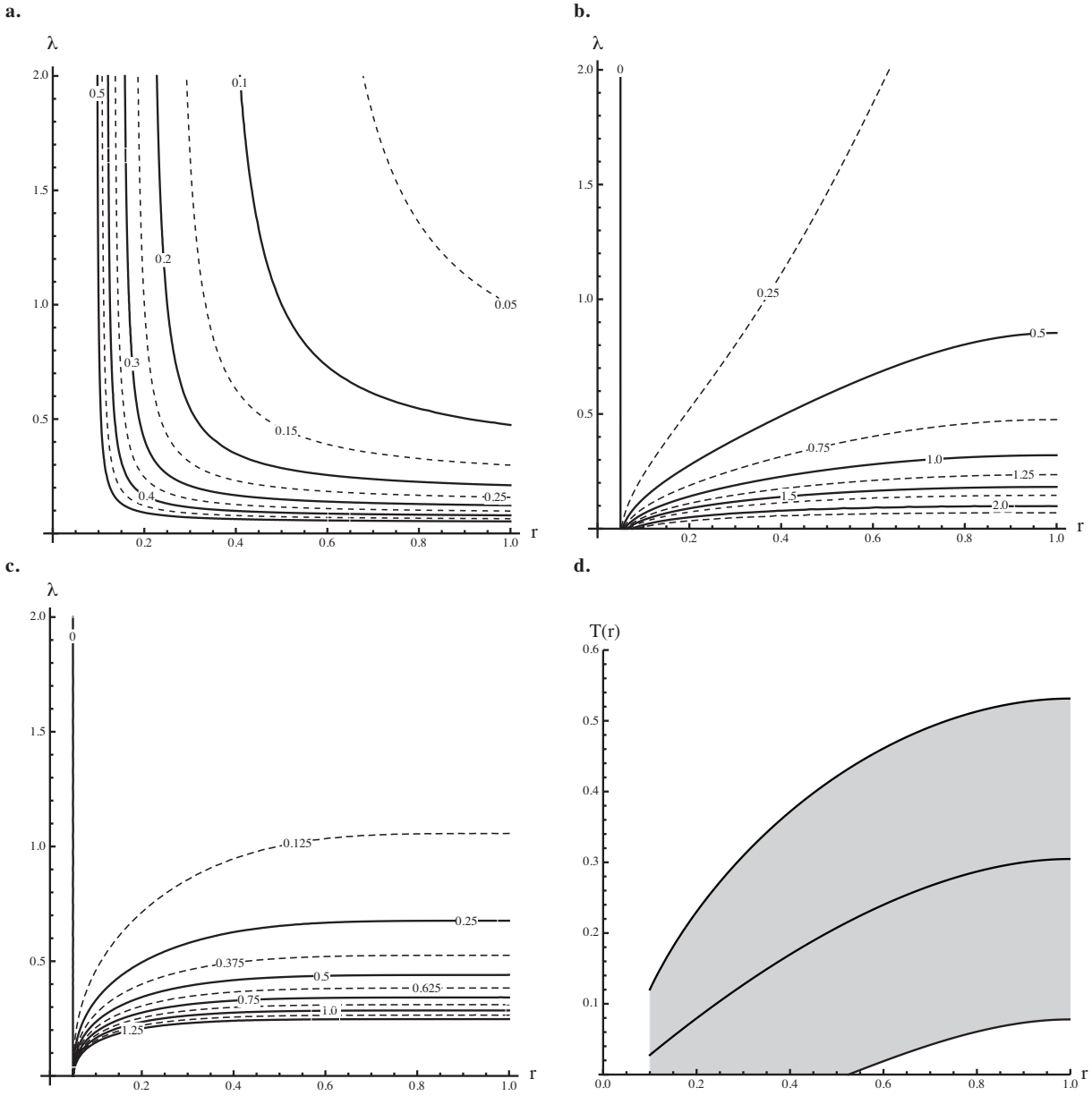

Figure 4. Splitting probability, conditional MFPT and conditional VFPT for spherically symmetric one-trap model with Robin boundary conditions. Space and time are rescaled so that the domain radius L and the diffusion coefficient D are eliminated from all expressions. **a.** Equally spaced contours of the probability of reaching the target $\mathbb{P}(r,\lambda)$ are plotted a single trap of radius 0.05 located at the sphere centre, as a function of r and λ. **b.** Equally spaced contours of the conditional mean first passage time to the target, $\mathbb{T}(r,\lambda)$. **c.** Equally spaced contours of the conditional variance of the first passage time to the target, $\mathbb{V}(r,\lambda)$. **d.** Mean $\pm$ standard deviation (shaded) conditional first passage time plotted against r for $\lambda = 2$, with central target size $a = 0.05$.

where c_j is the capacitance of Ω_j and $\mathbf{b}_j$ denotes the dipole vector, both determined by the shape of Ω_j. These intrinsic quantities can be found explicitly for different trap shapes such as spheres, ellipsoids, etc (see Table 1 of [**17**]). When Ω_{ε_j} is a sphere of radius εa_j, then Ω_j is a sphere of radius a_j, and we readily identify that $c_j = a_j$ and $\mathbf{b}_j = \mathbf{0}$. Upon using

the far-field asymptotic behavior (3.9 *b*) for w_{cj}, we obtain in terms of outer variables that

$$w_0 \sim \mathcal{P}_0 + (\delta_{j1} - \mathcal{P}_0)\left(\frac{\varepsilon c_j}{|\mathbf{x}-\mathbf{x}_j|} + \frac{\varepsilon^2 \mathbf{b}_j\cdot(\mathbf{x}-\mathbf{x}_j)}{|\mathbf{x}-\mathbf{x}_j|^3}\right), \quad \text{as} \quad |\mathbf{y}_j| \to \infty\,. \tag{3.10}$$

From (3.10) and (3.7), we conclude that $\mathcal{P}_1$ satisfies (3.4) with $k=1$ with singular behavior $\mathcal{P}_1 \sim (\delta_{j1}-\mathcal{P}_0)\,c_j/|\mathbf{x}-\mathbf{x}_j|$ as $\mathbf{x}\to\mathbf{x}_j$ for $j=1,\ldots,M$. Therefore, in terms of the Dirac distribution $\delta(\mathbf{x}-\mathbf{x}_i)$, we have that $\mathcal{P}_1$ satisfies

$$\Delta\mathcal{P}_1 = -4\pi c_1\,(1-\mathcal{P}_0)\,\delta(\mathbf{x}-\mathbf{x}_1) + 4\pi\mathcal{P}_0\sum_{i=2}^{M} c_i\delta(\mathbf{x}-\mathbf{x}_i)\,, \quad \mathbf{x}\in\Omega\,; \qquad \partial_n\mathcal{P}_1 = -\kappa\mathcal{P}_0\,, \quad \mathbf{x}\in\partial\Omega\,. \tag{3.11}$$

Upon applying the divergence theorem to (3.11), we obtain in terms of the surface area $|\partial\Omega|$ of $\partial\Omega$ that

$$\mathcal{P}_0 = \frac{4\pi c_1}{\gamma}\,, \qquad \gamma \equiv \kappa|\partial\Omega| + 4\pi M\bar{c}\,, \qquad \bar{c} \equiv \frac{1}{M}\sum_{i=1}^{M} c_i\,. \tag{3.12}$$

To solve (3.11) we introduce the unique Neumann Green's function $G(\mathbf{x};\xi)$ and its regular part $R(\xi)$ satisfying

$$\begin{aligned} &\Delta G = \frac{1}{|\Omega|} - \delta(\mathbf{x}-\xi)\,, \quad \mathbf{x}\in\Omega\,; \qquad \partial_n G = 0\,, \quad \mathbf{x}\in\partial\Omega\,,\\ &G(\mathbf{x};\xi) \sim \frac{1}{4\pi|\mathbf{x}-\xi|} + R(\xi) + o(1)\,, \quad \text{as } \mathbf{x}\to\xi\,; \qquad \int_\Omega G(\mathbf{x};\xi)\,d\mathbf{x} = 0\,, \end{aligned} \tag{3.13}$$

where $|\Omega|$ denotes the volume of Ω. In addition, we introduce the function $P_{1p}(\mathbf{x})$ defined uniquely by

$$\Delta P_{1p} = \frac{|\partial\Omega|}{|\Omega|}\,, \quad \mathbf{x}\in\Omega\,; \qquad \partial_n P_{1p} = 1\,, \quad \mathbf{x}\in\partial\Omega\,; \qquad \int_\Omega P_{1p}\,d\mathbf{x} = 0\,. \tag{3.14}$$

In terms of G, we use Green's second identity to get

$$P_{1p}(\mathbf{x}) = \int_{\partial\Omega} G(\xi;\mathbf{x})\,d\xi\,, \qquad \mathbf{x}\in\Omega\,. \tag{3.15}$$

To evaluate $P_{1p}(\mathbf{x}_b)$ for $\mathbf{x}_b\in\partial\Omega$ we can use a limiting process $P_{1p}(\mathbf{x}_b) = \lim_{\mathbf{x}\to\mathbf{x}_b}\int_{\partial\Omega} G(\xi;\mathbf{x})\,d\xi$.

In terms of G and P_{1p}, the solution to (3.11) can be decomposed as

$$\mathcal{P}_1(\mathbf{x}) = -\kappa\mathcal{P}_0 P_{1p}(\mathbf{x}) + 4\pi\sum_{i=1}^{M} c_i\,(\delta_{i1}-\mathcal{P}_0)\,G(\mathbf{x};\mathbf{x}_i) + \chi_1\,, \tag{3.16}$$

where $\chi_1 \equiv |\Omega|^{-1}\int_\Omega \mathcal{P}_1\,d\mathbf{x}$ is a constant to be found. To determine χ_1, we must proceed to one higher order in the analysis. To do so, we expand $\mathcal{P}_1$ as $\mathbf{x}\to\mathbf{x}_j$, to obtain

$$\mathcal{P}_1 \sim -\frac{c_j\mathcal{P}_0}{|\mathbf{x}-\mathbf{x}_j|} + \mathcal{P}_{1j} + \chi_1 + \cdots\,, \quad \text{as} \quad \mathbf{x}\to\mathbf{x}_j\,, \tag{3.17 a}$$

where $\mathcal{P}_{1j}$ is defined in terms of $R_j \equiv R(\mathbf{x}_j)$ and $G_{ji}\equiv G(\mathbf{x}_j;\mathbf{x}_i)$ by

$$\mathcal{P}_{1j} \equiv -\kappa\mathcal{P}_0 P_{1p}(\mathbf{x}_j) + 4\pi c_j\,(\delta_{j1}-\mathcal{P}_0)\,R_j + 4\pi\sum_{\substack{i=1\\ i\neq j}}^{M} c_i\,(\delta_{i1}-\mathcal{P}_0)\,G_{ji}\,, \quad j=1,\ldots,M\,. \tag{3.17 b}$$

By substituting (3.17 *a*) into the matching condition (3.7), we conclude that $w_1 \sim \mathcal{P}_{1j}+\chi_1$ as $|\mathbf{y}_j|\to\infty$. The solution to (3.6 *b*) with this far-field behavior is $w_1 = (\mathcal{P}_{1j}+\chi_1)\,(1-w_{cj})$, where w_{cj} satisfies (3.9 *a*). Upon using the far-field behavior (3.9 *b*), we calculate that

$$w_1 \sim (\mathcal{P}_{1j}+\chi_1)\left(1 - \frac{\varepsilon c_j}{|\mathbf{x}-\mathbf{x}_j|} + \cdots\right), \qquad \text{as} \quad |\mathbf{y}_j|\to\infty\,. \tag{3.18}$$

Then, upon substituting (3.18) and (3.9 b) into the matching condition (3.7), we obtain that $\mathcal{P}_2$ satisfies (3.4) with $k=2$ subject to the singularity behavior

$$\mathcal{P}_2 \sim (\delta_{j1}-\mathcal{P}_0)\,\frac{\mathbf{b}_j\cdot(\mathbf{x}-\mathbf{x}_j)}{|\mathbf{x}-\mathbf{x}_j|^3}-\frac{c_j\,(\mathcal{P}_{1j}+\chi_1)}{|\mathbf{x}-\mathbf{x}_j|}\,, \qquad \text{as} \quad \mathbf{x}\to\mathbf{x}_j\,. \tag{3.19}$$

This problem for $\mathcal{P}_2$ is equivalent to

$$\Delta\mathcal{P}_2 = 4\pi\sum_{i=1}^{M}\left[c_i\,(\mathcal{P}_{1i}+\chi_1)\;\delta(\mathbf{x}-\mathbf{x}_i)+(\delta_{i1}-\mathcal{P}_0)\,\mathbf{b}_i\cdot\nabla_{\mathbf{x}}\delta(\mathbf{x}-\mathbf{x}_i)\right]\,, \quad \mathbf{x}\in\Omega\,; \qquad \partial_n\mathcal{P}_2=-\kappa\mathcal{P}_1\,, \quad \mathbf{x}\in\partial\Omega\,. \tag{3.20}$$

The divergence theorem yields that $4\pi\sum_{i=1}^{M}c_i\,(\mathcal{P}_{1i}+\chi_1)=-\kappa\int_{\partial\Omega}\mathcal{P}_1\,d\mathbf{x}$, which is independent of the dipole vectors $\mathbf{b}_i$ for $i=1,\dots,M$. By using (3.17 b) for $\mathcal{P}_{1i}$ we get

$$\chi_1+\frac{\kappa}{4\pi M\bar{c}}\int_{\partial\Omega}\mathcal{P}_1\,d\mathbf{x}=-\frac{1}{M\bar{c}}\sum_{i=1}^{M}c_i\mathcal{P}_{1i}=\frac{\kappa\mathcal{P}_0}{M\bar{c}}\mathbf{c}^T\mathbf{P}_{1p}-\frac{4\pi c_1}{M\bar{c}}\left[(\mathcal{G}\mathbf{c})_1-\frac{\mathcal{P}_0}{c_1}\mathbf{c}^T\mathcal{G}\mathbf{c}\right]\,, \tag{3.21}$$

where we have defined the capacitance vector $\mathbf{c}$, the vector $\mathbf{P}_{1p}$, and the Green's matrix $\mathcal{G}$ by

$$\mathbf{c}\equiv\begin{pmatrix}c_1\\ \vdots\\ c_M\end{pmatrix}\,, \qquad \mathbf{P}_{1p}\equiv\begin{pmatrix}P_{1p}(\mathbf{x}_1)\\ \vdots\\ P_{1p}(\mathbf{x}_M)\end{pmatrix}\,, \qquad \mathcal{G}\equiv\begin{pmatrix}R_1 & G_{1,2} & \cdots & G_{1,M}\\ G_{2,1} & \ddots & \ddots & \vdots\\ \vdots & \ddots & \ddots & G_{M-1,M}\\ G_{M,1} & \cdots & G_{M,M-1} & R_M\end{pmatrix}\,. \tag{3.22}$$

In (3.21), $(\mathcal{G}\mathbf{c})_1$ denotes the first entry of the vector $\mathcal{G}\mathbf{c}$.

To calculate the boundary integral on the left-hand side of (3.21), we use (3.16) to obtain

$$\int_{\partial\Omega}\mathcal{P}_1\,d\mathbf{x}=-\kappa\mathcal{P}_0\int_{\partial\Omega}P_{1p}\,d\mathbf{x}+4\pi\sum_{i=1}^{M}c_1\,(\delta_{i1}-\mathcal{P}_0)\int_{\partial\Omega}G(\mathbf{x};\mathbf{x}_i)\,d\mathbf{x}+\chi_1|\partial\Omega|\,,$$

where we identify $\int_{\partial\Omega}G(\mathbf{x};\mathbf{x}_i)\,d\mathbf{x}=P_{1p}(\mathbf{x}_i)$ from (3.15). Upon substituting this expression into (3.21) we obtain an algebraic equation for χ_1 that is readily solved. This leads to the following main result.

Principal Result 3.1: *In the limit $\varepsilon\to 0$, the splitting probability $\mathcal{P}$ satisfying (3.1) with $\lambda=\varepsilon\kappa$, is given asymptotically in the outer region $|\mathbf{x}-\mathbf{x}_j|\gg\mathcal{O}(\varepsilon)$ for $j=1,\dots,M$ by*

$$\mathcal{P}\sim\mathcal{P}_0+\varepsilon\mathcal{P}_1+\cdots=\frac{4\pi c_1}{\gamma}+\varepsilon\left[-\kappa\mathcal{P}_0P_{1p}(\mathbf{x})+4\pi\sum_{i=1}^{M}c_i\,(\delta_{i1}-\mathcal{P}_0)\,G(\mathbf{x};\mathbf{x}_i)+\chi_1\right]+\cdots\,. \tag{3.23 a}$$

Here γ and $\mathcal{P}_0$ are defined in (3.12), and χ_1 is given by

$$\chi_1=\mathcal{P}_0\left(\frac{2\kappa\mathcal{P}_0}{c_1}\mathbf{c}^T\mathbf{P}_{1p}-\kappa P_{1p}(\mathbf{x}_1)+\frac{\kappa^2\mathcal{P}_0}{4\pi c_1}\int_{\partial\Omega}P_{1p}(\mathbf{x})\,d\mathbf{x}-4\pi\left[(\mathcal{G}\mathbf{c})_1-\frac{\mathcal{P}_0}{c_1}\mathbf{c}^T\mathcal{G}\mathbf{c}\right]\right)\,. \tag{3.23 b}$$

In (3.23 b) the Green's matrix $\mathcal{G}$, the capacitance vector $\mathbf{c}$, and the vector $\mathbf{P}_{1p}$ are defined in (3.22). The Neumann Green's function G and the function P_{1p} are defined by (3.13) and (3.14), respectively.

For a perfectly reflecting boundary where $\kappa=0$, the result in (3.23) reduces to that obtained in Principal Result 3.2 of [**17**]. When the boundary is slightly sticky with $\lambda=\varepsilon\kappa>0$, we observe (as anticipated) that the leading-order splitting probability $\mathcal{P}_0$ is smaller than when $\kappa=0$. For the regime $\mathcal{O}(1)\ll\kappa\ll\mathcal{O}(\varepsilon^{-1})$, we readily calculate from (3.23) that

$$\mathcal{P}\sim\frac{4\pi c_1}{\kappa|\partial\Omega|}-\frac{16\pi^2c_1M\bar{c}}{\kappa^2|\partial\Omega|^2}+\varepsilon\left[-\frac{4\pi c_1}{|\partial\Omega|}P_{1p}(\mathbf{x})+4\pi c_1G(\mathbf{x};\mathbf{x}_1)+\frac{4\pi c_1}{|\partial\Omega|^2}\int_{\partial\Omega}P_{1p}\,d\mathbf{x}-\frac{4\pi c_1P_{1p}(\mathbf{x}_1)}{|\partial\Omega|}\right]\,. \tag{3.24}$$

This result is re-derived below in §3.1 after calculating the splitting probability for a strongly sticky boundary where $\lambda = \mathcal{O}(1)$.

We now apply Principal Result 3.1 to the case where Ω is a sphere of radius L. Then, as derived in Appendix A of [**17**], the Neumann Green's function satisfying (3.13) is given explicitly by

$$G(\mathbf{x};\xi) = \frac{1}{4\pi|\mathbf{x}-\xi|} + \frac{L}{4\pi|\mathbf{x}||\mathbf{x}'-\xi|} + \frac{1}{4\pi L}\log\left(\frac{2L^2}{L^2 - |\mathbf{x}||\xi|\cos\theta + |\mathbf{x}||\mathbf{x}'-\xi|}\right) + \frac{\left(|\mathbf{x}|^2+|\xi|^2\right)}{8\pi L^3} - \frac{7}{10\pi L}\,. \tag{3.25 a}$$

Here $\mathbf{x}' = \mathbf{x}L^2/|\mathbf{x}|^2$ is the image point to $\mathbf{x}$ outside the sphere, and θ is the angle between ξ and $\mathbf{x}$, i.e. $\cos\theta = \mathbf{x}\cdot\xi/|\mathbf{x}||\xi|$, where $\cdot$ denotes the dot product. The regular part $R(\xi)$ of this Green's function is

$$R(\xi) = \frac{L}{4\pi\left[L^2 - |\xi|^2\right]} + \frac{1}{4\pi L}\log\left(\frac{L^2}{L^2-|\xi|^2}\right) + \frac{|\xi|^2}{4\pi L^3} - \frac{7}{10\pi L}\,. \tag{3.25 b}$$

For the radially symmetric case where $\xi = \mathbf{0}$, then (3.25 *a*) and (3.25 *b*) reduce to

$$G(\mathbf{x};\mathbf{0}) = \frac{1}{4\pi|\mathbf{x}|} + \frac{|\mathbf{x}|^2}{8\pi L^3} - \frac{9}{20\pi L}\,, \qquad R(\mathbf{0}) = -\frac{9}{20\pi L}\,. \tag{3.26}$$

In addition, when Ω is a sphere of radius L, then $\mathcal{P}_0$ from (3.12) and the solution P_{1p} to (3.14) are

$$\mathcal{P}_0 = \frac{c_1}{\kappa L^2 + M\bar{c}}\,, \qquad P_{1p}(\mathbf{x}) = \frac{|\mathbf{x}|^2}{2L} - \frac{3L}{10}\,, \tag{3.27}$$

while from (3.23 *b*) we get

$$\chi_1 = \mathcal{P}_0\left[\frac{\kappa\mathcal{P}_0}{c_1 L}\sum_{i=1}^{M} c_i|\mathbf{x}_i|^2 - \frac{3\kappa\mathcal{P}_0}{5c_1}LM\bar{c} + \frac{\kappa^2\mathcal{P}_0 L^3}{5c_1} - \frac{\kappa|\mathbf{x}_1|^2}{2L} + \frac{3L\kappa}{10} - 4\pi\left(\left(\mathcal{G}\mathbf{c}\right)_1 - \frac{\mathcal{P}_0}{c_1}\mathbf{c}^T\mathcal{G}\mathbf{c}\right)\right]. \tag{3.28}$$

Finally, if the M small traps Ω_{ε_j} for $j = 1,\ldots,M$ are non-overlapping spheres of radii εa_j centered at $\mathbf{x}_j \in \Omega$ for $j = 1,\ldots,M$, then we simply set $c_j = a_j$ in (3.28).

For the simple concentric radially symmetric case of one trap of radius ε centered at the origin of a sphere of radius L, so that $c_1 = 1$, we have from (3.23 *a*) that

$$\mathcal{P} \sim \mathcal{P}_0 + \varepsilon\left[-\kappa\mathcal{P}_0 P_{1p} + 4\pi\left(1-\mathcal{P}_0\right)G(r;\mathbf{0}) + \chi_1\right], \tag{3.29}$$

where $\mathcal{P}_0 = 1/(\kappa L^2+1)$. From (3.28), we get

$$\chi_1 = \mathcal{P}_0\left[-\frac{3\kappa\mathcal{P}_0 L}{5} + \frac{\kappa^2\mathcal{P}_0 L^3}{5} + \frac{3L\kappa}{10} - 4\pi R(\mathbf{0})\left(1-\mathcal{P}_0\right)\right]. \tag{3.30}$$

Upon substituting (3.26) and (3.27) into (3.29) and (3.30) we obtain, after some algebra, that

$$\mathcal{P} \sim \mathcal{P}_0 + \varepsilon\left[\frac{(1-\mathcal{P}_0)}{|\mathbf{x}|} - \mathcal{P}_0^2\kappa^2 L^3\right]. \tag{3.31}$$

We can readily recover (3.31) from the exact result given in (2.15 *a*) for the concentric domain $\varepsilon \le |\mathbf{x}| \le L$. If we set $a = \varepsilon$ and $\lambda = \varepsilon\kappa$ in (2.15 *a*) and then expand for $\varepsilon \to 0$, we readily obtain (3.31).

3.1 A Strongly Sticky Boundary

A similar matched asymptotic analysis can be done for (3.1) when $\lambda = \mathcal{O}(1)$. For this case, the probability of reaching the target trap Ω_{ε_1} first is only $\mathcal{O}(\varepsilon)$ when $|\mathbf{x}-\mathbf{x}_1| = \mathcal{O}(1)$. In the outer region we now expand $\mathcal{P}$ as

$$\mathcal{P} = \varepsilon\mathcal{P}_0 + \varepsilon^2\mathcal{P}_1 + \cdots\,. \tag{3.32}$$

Upon substituting this expansion into (3.1 a), we obtain for $k = 0, 1$ that

$$\Delta \mathcal{P}_k = 0\,, \qquad \mathbf{x} \in \Omega \backslash \{\mathbf{x}_1, \ldots, \mathbf{x}_M\}\,; \qquad \partial_n \mathcal{P}_k + \lambda \mathcal{P}_k = 0\,, \qquad \mathbf{x} \in \partial\Omega\,, \tag{3.33}$$

with certain singularity conditions as $\mathbf{x} \to \mathbf{x}_j$ for $j = 1, \ldots, M$ to be determined.

In the inner region near the target trap, we write $w(\mathbf{y}_1) \equiv \mathcal{P}(\mathbf{x}_1 + \varepsilon \mathbf{y}_1)$, with $\mathbf{y}_1 \equiv \varepsilon^{-1}(\mathbf{x} - \mathbf{x}_1)$, and expand

$$w = w_0 + \varepsilon w_1 + \cdots\,. \tag{3.34}$$

Upon substituting (3.34) into (3.1 b) and the PDE of (3.1 a), we obtain that w_0 and w_1 satisfy

$$\Delta_y w_0 = 0\,, \quad \mathbf{y}_1 \notin \Omega_1\,; \qquad w_0 = 1\,, \quad \mathbf{y}_1 \in \partial\Omega_1\,, \tag{3.35 a}$$

$$\Delta_y w_1 = 0\,, \quad \mathbf{y}_1 \notin \Omega_1\,; \qquad w_1 = 0\,, \quad \mathbf{y}_1 \in \partial\Omega_1\,. \tag{3.35 b}$$

The matching condition as $\mathbf{x} \to \mathbf{x}_1$ and $|\mathbf{y}_1| \to \infty$ is that

$$\varepsilon \mathcal{P}_0 + \varepsilon^2 \mathcal{P}_1 + \cdots \sim w_0 + \varepsilon w_1 + \cdots\,. \tag{3.36}$$

The leading order matching condition is that $w_0 \to 0$ as $|\mathbf{y}_1| \to \infty$. From (3.35 a), we conclude that $w_0 = w_{c1}$, where w_{c1} satisfies (3.9 a) with $j = 1$. Hence, by using (3.9 b), and writing the result in outer variables, we obtain that

$$w_0 \sim \frac{\varepsilon c_1}{|\mathbf{x} - \mathbf{x}_1|} + \frac{\varepsilon^2 \mathbf{b}_1 \cdot (\mathbf{x} - \mathbf{x}_1)}{|\mathbf{x} - \mathbf{x}_1|^3} + \cdots \qquad \text{as} \quad |\mathbf{y}_1| \to \infty\,. \tag{3.37}$$

From the matching condition (3.36) this yields that

$$\mathcal{P}_0 \sim \frac{c_1}{|\mathbf{x} - \mathbf{x}_1|}\,, \qquad \text{as} \quad \mathbf{x} \to \mathbf{x}_1\,. \tag{3.38}$$

Since $\mathcal{P} = \mathcal{O}(\varepsilon)$ in the outer region, while $\mathcal{P} = 0$ on the boundary of each of the $M - 1$ non-target traps, we have that $w = \mathcal{O}(\varepsilon)$ in the inner region near these traps. Therefore, for the non-target traps, we pose a modified inner expansion

$$w = \varepsilon w_1 + \varepsilon^2 w_2 + \cdots\,, \tag{3.39}$$

so that for $j = 2, \ldots, M$, we have

$$\Delta_y w_1 = 0\,, \quad \mathbf{y}_1 \notin \Omega_j\,; \qquad w_1 = 0\,, \quad \mathbf{y}_1 \in \partial\Omega_j\,. \tag{3.40}$$

The matching condition for $j = 2, \ldots, M$ when $\mathbf{x} \to \mathbf{x}_j$ and $|\mathbf{y}_j| \to \infty$ is that

$$\varepsilon \mathcal{P}_0 + \varepsilon^2 \mathcal{P}_1 + \cdots \sim \varepsilon w_1 + \varepsilon^2 w_2 + \cdots\,. \tag{3.41}$$

The leading-order matching condition is that $w_1 \to \mathcal{P}_0(\mathbf{x}_j)$ as $|\mathbf{y}_j| \to \infty$ for $j = 2, \ldots, N$. The solution is $w_1 = \mathcal{P}_0(\mathbf{x}_j)(1 - w_{cj})$, which yields the far-field behavior

$$\varepsilon w_1 \sim \varepsilon \mathcal{P}_0(\mathbf{x}_j) \left(1 - \frac{\varepsilon c_j}{|\mathbf{x} - \mathbf{x}_j|} + \cdots\right)\,, \qquad \text{as} \quad |\mathbf{y}_j| \to \infty\,, \quad j = 2, \ldots, M\,, \tag{3.42}$$

when written in outer variables. From the matching condition (3.41), we conclude that

$$\mathcal{P}_1 \sim -\frac{\mathcal{P}_0(\mathbf{x}_j) c_j}{|\mathbf{x} - \mathbf{x}_j|}\,, \qquad \text{as} \quad \mathbf{x} \to \mathbf{x}_j\,, \quad \text{for} \quad j = 2, \ldots, M\,. \tag{3.43}$$

We conclude that $\mathcal{P}_0$ satisfies (3.33) with $k = 0$, subject to the singularity behavior (3.38) as $\mathbf{x} \to \mathbf{x}_1$, while $\mathcal{P}_0$ has no singularity at $\mathbf{x}_j$ for $j = 2, \ldots, M$. The solution to this problem is

$$\mathcal{P}_0 = 4\pi c_1 G_\lambda(\mathbf{x}; \mathbf{x}_1)\,, \tag{3.44}$$

where $G_\lambda(\mathbf{x};\xi)$ is the Green's function, with regular part $R_\lambda(\xi)$, satisfying

$$\Delta G_\lambda = -\delta(\mathbf{x}-\xi)\,, \quad \mathbf{x}\in\Omega\,; \qquad \partial_n G_\lambda + \lambda G_\lambda = 0\,, \quad \mathbf{x}\in\partial\Omega\,; \qquad G_\lambda(\mathbf{x};\xi)\sim \frac{1}{4\pi|\mathbf{x}-\xi|} + R_\lambda(\xi)\,, \quad \text{as } \mathbf{x}\to\xi\,. \tag{3.45}$$

By expanding $\mathcal{P}_0$ as $\mathbf{x}\to\mathbf{x}_1$ we obtain from the matching condition (3.36) for the target trap that

$$w_1 \sim 4\pi c_1 R_\lambda(\mathbf{x}_1)\,, \quad \text{as} \quad |\mathbf{y}_1|\to\infty\,. \tag{3.46}$$

The solution to (3.35 b) with this behavior is $w_1 = 4\pi c_1 R_\lambda(\mathbf{x}_1)(1-w_{c1})$. Next, we use the far-field behavior (3.9 b) of w_{c1} to obtain in terms of outer variables that

$$\varepsilon w_1 \sim 4\pi\varepsilon c_1 R_\lambda(\mathbf{x}_1) - \frac{4\pi\varepsilon^2 c_1^2}{|\mathbf{x}-\mathbf{x}_1|}R_\lambda(\mathbf{x}_1)\,, \quad \text{as} \quad |\mathbf{y}_1|\to\infty\,. \tag{3.47}$$

We substitute (3.47) and (3.37) into the matching condition (3.36), and then identify the $\mathcal{O}(\varepsilon^2)$ term to obtain the following singularity behavior for $\mathcal{P}_1$ at the target trap:

$$\mathcal{P}_1 \sim -\frac{4\pi c_1^2}{|\mathbf{x}-\mathbf{x}_1|}R_\lambda(\mathbf{x}_1) + \frac{\mathbf{b}_1\cdot(\mathbf{x}-\mathbf{x}_1)}{|\mathbf{x}-\mathbf{x}_1|^3}\,, \qquad \text{as} \quad \mathbf{x}\to\mathbf{x}_1\,. \tag{3.48}$$

For the non-target traps, the singularity behavior of $\mathcal{P}_1$ is (3.43) where $\mathcal{P}_0(\mathbf{x}_j) = 4\pi c_1 G_\lambda(\mathbf{x}_j;\mathbf{x}_1)$.

The problem (3.33) with $k=1$ for $\mathcal{P}_1$ with singularity behavior (3.48) and (3.43) at the target and non-target traps, respectively, can be written in terms of the Dirac delta function as

$$\begin{aligned} &\Delta\mathcal{P}_1 = 16\pi^2 c_1^2 R_\lambda(\mathbf{x}_1)\delta(\mathbf{x}-\mathbf{x}_1) - 4\pi\mathbf{b}_1\cdot\nabla_{\mathbf{x}_1}\delta(\mathbf{x}-\mathbf{x}_1) + 4\pi\sum_{i=2}^{M} c_i\mathcal{P}_0(\mathbf{x}_i)\delta(\mathbf{x}-\mathbf{x}_i)\,, \quad \mathbf{x}\in\Omega\,, \\ &\partial_n\mathcal{P}_1 + \lambda\mathcal{P}_1 = 0\,, \qquad \mathbf{x}\in\partial\Omega\,. \end{aligned} \tag{3.49}$$

The solution to (3.49) can be written in terms of G_λ. We summarize our result as follows.

Principal Result 3.2: *In the limit $\varepsilon\to 0$, the splitting probability $\mathcal{P}$ satisfying (3.1) with $\lambda = \mathcal{O}(1)$ is given asymptotically in the outer region $|\mathbf{x}-\mathbf{x}_j|\gg\mathcal{O}(\varepsilon)$ for $j=1,\dots,M$ by*

$$\mathcal{P}\sim 4\pi\varepsilon c_1 G_\lambda(\mathbf{x};\mathbf{x}_1) + \varepsilon^2\left[-16\pi^2 c_1^2 R_\lambda(\mathbf{x}_1)G_\lambda(\mathbf{x};\mathbf{x}_1) + 4\pi\mathbf{b}_1\cdot\nabla_{\mathbf{x}_1}G_\lambda(\mathbf{x};\mathbf{x}_1) - 16\pi^2 c_1\sum_{i=2}^{M} c_i G_\lambda(\mathbf{x}_i;\mathbf{x}_1)G_\lambda(\mathbf{x};\mathbf{x}_i)\right]. \tag{3.50}$$

In (3.50) the Green's function G_λ and its regular part R_λ satisfy (3.45).

Finally, we let $\lambda\ll 1$ in (3.50) and we show that (3.50) makes a uniformly valid transition to the result given in (3.24) for a slightly sticky boundary when $\kappa\gg 1$. We assume that $\mathcal{O}(\varepsilon)\ll\lambda\ll\mathcal{O}(1)$. For $\lambda\ll 1$ we calculate G_λ from (3.45) by expanding $G_\lambda\sim A\lambda^{-1} + \hat{G}_0 + \lambda\hat{G}_1 + \cdots$. We substitute this expansion into (3.45) and collect powers of λ to get

$$\Delta\hat{G}_0 = -\delta(\mathbf{x}-\xi)\,, \quad \mathbf{x}\in\Omega\,; \qquad \partial_n\hat{G}_0 = -A\,, \quad \mathbf{x}\in\partial\Omega\,. \tag{3.51}$$

From the $\hat{G}_1$ problem we must impose that $\int_{\partial\Omega}\hat{G}_0\,d\mathbf{x} = 0$. The divergence theorem then yields $A = 1/|\partial\Omega|$. The solution to (3.51) is readily calculated in terms of an arbitrary constant μ as

$$\hat{G}_0(x;\xi) = G(\mathbf{x};\xi) - \frac{1}{|\partial\Omega|}P_{1p}(\mathbf{x}) + \mu\,, \tag{3.52}$$

where $G(\mathbf{x};\xi)$ is the Neumann Green's function of (3.13) and $P_{1p}(\mathbf{x})$ is the solution to (3.14). The constant μ is determined from the condition $\int_{\partial\Omega}\hat{G}_0\,d\mathbf{x} = 0$. In this way, we obtain for $\lambda\ll 1$ that

$$G_\lambda(\mathbf{x};\xi)\sim\frac{1}{\lambda|\partial\Omega|} + G(\mathbf{x};\xi) - \frac{1}{|\partial\Omega|}P_{1p}(\mathbf{x}) - \frac{1}{|\partial\Omega|}P_{1p}(\xi) + \frac{1}{|\partial\Omega|^2}\int_{\partial\Omega}P_{1p}\,d\mathbf{x}\,. \tag{3.53}$$

Finally, upon substituting (3.53) and $R_\lambda \sim 1/(\lambda|\Omega|)$ into (3.50), we obtain for $\mathcal{O}(\varepsilon) \ll \lambda \ll \mathcal{O}(1)$ that

$$\mathcal{P} \sim \frac{4\pi c_1 \varepsilon}{\lambda|\partial\Omega|} - \frac{16\pi^2\varepsilon^2 c_1 M\bar{c}}{\lambda^2|\partial\Omega|^2} + \varepsilon\left[-\frac{4\pi c_1}{|\partial\Omega|}P_{1p}(\mathbf{x}) + 4\pi c_1 G(\mathbf{x};\mathbf{x}_1) + \frac{4\pi c_1}{|\partial\Omega|^2}\int_{\partial\Omega} P_{1p}\,d\mathbf{x} - \frac{4\pi c_1 P_{1p}(\mathbf{x}_1)}{|\partial\Omega|}\right]. \tag{3.54}$$

Upon replacing λ by $\lambda = \varepsilon\kappa$ in (3.54) we recover (3.24). Therefore, the result in Principal Result 3.2 provides a uniformly valid transition to that in Principal Result 3.1 when λ satisfies $\mathcal{O}(\varepsilon) \ll \lambda \ll \mathcal{O}(1)$.

4 Conditional Mean First Passage Time

In this section we calculate the mean first passage time (MFPT) conditional on the diffusing particle reaching the target Ω_{ε_1}. Assuming a weakly sticky boundary, this conditional MFPT satisfies

$$\Delta[\mathcal{P}\mathbb{T}] = -\frac{\mathcal{P}}{D}, \quad \mathbf{x}\in\Omega\backslash\Omega_p; \qquad \partial_n[\mathcal{P}\mathbb{T}] + \varepsilon\kappa[\mathcal{P}\mathbb{T}] = 0, \quad \mathbf{x}\in\partial\Omega, \tag{4.1 a}$$

$$\mathcal{P}\mathbb{T} = 0, \quad \mathbf{x}\in\partial\Omega_{\epsilon_1}; \qquad \mathcal{P}\mathbb{T}\to 0, \quad \mathbf{x}\in\partial\Omega_{\epsilon_j}, \quad j = 2,\dots,M. \tag{4.1 b}$$

Here $\mathcal{P}$ is the splitting probability satisfying (3.1) when $\lambda = \varepsilon\kappa$, as given asymptotically in Principal Result 3.1. Since $\mathcal{P} = 0$ on $\partial\Omega_{\varepsilon_j}$ for $j = 2,\dots,M$, the condition in (4.1 *b*) on the non-target traps is a boundedness condition on $\mathbb{T}$.

To analyze (4.1), it is convenient to define a new variable $\mathcal{U}$ by

$$\mathbb{T} = \mathcal{U}/\mathcal{P}, \tag{4.2}$$

so that from (4.1), $\mathcal{U}$ satisfies

$$\Delta\mathcal{U} = -\frac{\mathcal{P}}{D}, \qquad \mathbf{x}\in\Omega\backslash\Omega_p; \qquad \partial_n\mathcal{U} + \varepsilon\kappa\mathcal{U} = 0, \qquad \mathbf{x}\in\partial\Omega, \tag{4.3 a}$$

$$\mathcal{U} = 0, \quad \mathbf{x}\in\partial\Omega_{\epsilon_1}; \qquad \mathcal{U}\to 0, \quad \mathbf{x}\in\partial\Omega_{\epsilon_j}, \quad j = 2,\dots,M. \tag{4.3 b}$$

As a remark, if we set $\mathcal{P}\equiv 1$ in (4.3 *a*) then $\mathcal{U}$ is the MFPT for a diffusing particle to be captured at any one of the traps or on the sticky boundary. This observation is exploited below in §5.

We now solve (4.3) by the method of matched asymptotic expansions. In the outer region, defined at $\mathcal{O}(1)$ distances away from the traps, we expand $\mathcal{U}$ as

$$\mathcal{U} = \varepsilon^{-1}\mathcal{U}_0 + \mathcal{U}_1 + \varepsilon\mathcal{U}_2 + \cdots, \tag{4.4}$$

where $\mathcal{U}_0$ is an unknown constant. We expand $\mathcal{P} = \mathcal{P}_0 + \varepsilon\mathcal{P}_1 + \cdots$ and use (4.3 *a*), to obtain that $\mathcal{U}_k$ for $k = 1, 2$ satisfies

$$\Delta\mathcal{U}_k = -\frac{\mathcal{P}_{k-1}}{D}, \qquad \mathbf{x}\in\Omega\backslash\{\mathbf{x}_1,\dots,\mathbf{x}_M\}; \qquad \partial_n\mathcal{U}_k = -\kappa\mathcal{U}_{k-1}, \qquad \mathbf{x}\in\partial\Omega, \tag{4.5}$$

subject to singularity conditions as $\mathbf{x}\to\mathbf{x}_j$ for $j = 1,\dots,M$ that are to be determined.

In the inner region near the j-th trap, we write $u(\mathbf{y}_j) \equiv \mathcal{U}(\mathbf{x}_j + \varepsilon\mathbf{y}_j)$, with $\mathbf{y}_j \equiv \varepsilon^{-1}(\mathbf{x} - \mathbf{x}_j)$, and expand

$$u = \varepsilon^{-1}u_0 + u_1 + \varepsilon u_2 + \cdots. \tag{4.6}$$

Upon substituting (4.6) into (4.3 *b*) and the PDE of (4.3 *a*), we obtain that u_k for $k = 0, 1$ satisfies

$$\Delta_y u_k = 0, \quad \mathbf{y}_j\notin\Omega_j; \qquad u_k = 0, \quad \mathbf{y}_j\in\partial\Omega_j, \tag{4.7}$$

for $j = 1,\dots,M$. The matching condition between the inner and outer solutions is that

$$\varepsilon^{-1}\mathcal{U}_0 + \mathcal{U}_1 + \varepsilon\mathcal{U}_2 + \cdots \sim \varepsilon^{-1}u_0 + u_1 + \varepsilon u_2 + \cdots, \tag{4.8}$$

as $\mathbf{x}\to\mathbf{x}_j$ and $|\mathbf{y}_j|\to\infty$, for each $j = 1,\dots,M$.

The leading order matching condition is $u_0 \to \mathcal{U}_0$ as $|\mathbf{y}_j| \to \infty$. We conclude from (4.7) that $u_0 = \mathcal{U}_0(1 - w_{cj})$, where w_{cj} satisfies (3.9 *a*). From (3.9 *b*), the far-field behavior of u_0, when written in outer variables, is

$$u_0 \sim \mathcal{U}_0 \left(1 - \frac{\varepsilon c_j}{|\mathbf{x} - \mathbf{x}_j|} - \frac{\varepsilon^2 \mathbf{b}_j \cdot (\mathbf{x} - \mathbf{x}_j)}{|\mathbf{x} - \mathbf{x}_j|^3} + \cdots \right) \qquad \text{as} \quad |\mathbf{y}_j| \to \infty \,. \tag{4.9}$$

The matching condition (4.8) then yields that $\mathcal{U}_1 \sim -c_j \mathcal{U}_0 / |\mathbf{x} - \mathbf{x}_j|$ as $\mathbf{x} \to \mathbf{x}_j$. From (4.5) with $k = 1$, we get that

$$\Delta \mathcal{U}_1 = -\frac{\mathcal{P}_0}{D} + 4\pi \mathcal{U}_0 \sum_{i=i}^{M} c_i \delta(\mathbf{x} - \mathbf{x}_i) \,, \quad \mathbf{x} \in \Omega \,; \qquad \partial_n \mathcal{U}_1 = -\kappa \mathcal{U}_0 \,, \quad \mathbf{x} \in \partial\Omega \,. \tag{4.10}$$

Upon applying the divergence theorem to (4.10), and recalling (3.12) for $\mathcal{P}_0$, we calculate $\mathcal{U}_0$ as

$$\mathcal{U}_0 = \frac{\mathcal{P}_0 |\Omega|}{D\gamma} = \frac{4\pi c_1 |\Omega|}{D\gamma^2} \,, \qquad \gamma \equiv \kappa |\partial\Omega| + 4\pi M \bar{c} \,. \tag{4.11}$$

The solution to (4.10) is decomposed in terms of G and P_{1p}, satisfying (3.13) and (3.14), as

$$\mathcal{U}_1(\mathbf{x}) = -4\pi \mathcal{U}_0 \sum_{i=1}^{M} c_i G(\mathbf{x}; \mathbf{x}_i) - \kappa \mathcal{U}_0 P_{1p}(\mathbf{x}) + \bar{\mu}_1 \,, \tag{4.12}$$

where $\bar{\mu}_1 \equiv |\Omega|^{-1} \int_\Omega \mathcal{U}_1 \, d\mathbf{x}$ is a constant to be found. The constant $\bar{\mu}_1$ is calculated in Appendix A from a solvability condition on the problem for $\mathcal{U}_2$. This leads to the following main result:

Principal Result 4.1: *In the limit $\varepsilon \to 0$, the solution $\mathcal{U}$ to (4.3) is given asymptotically in the outer region $|\mathbf{x} - \mathbf{x}_j| \gg \mathcal{O}(\varepsilon)$ for $j = 1, \ldots, M$ by*

$$\mathcal{U} \sim \frac{\mathcal{U}_0}{\varepsilon} + \mathcal{U}_1 + \cdots = \frac{4\pi c_1 |\Omega|}{D\gamma^2 \varepsilon} + \left(-4\pi \mathcal{U}_0 \sum_{i=1}^{M} c_i G(\mathbf{x}; \mathbf{x}_i) - \kappa \mathcal{U}_0 P_{1p}(\mathbf{x}) + \bar{\mu}_1 \right) + \cdots \,. \tag{4.13 a}$$

Here γ is defined in (4.11) and $\bar{\mu}_1$ is given by

$$\bar{\mu}_1 = \frac{4\pi \mathcal{U}_0}{\gamma} \left[4\pi \mathbf{c}^T \mathcal{G} \mathbf{c} + 2\kappa \mathbf{c}^T \mathbf{P}_{1p} + \frac{\kappa^2}{4\pi} \int_{\partial\Omega} P_{1p} \, d\mathbf{x} + \frac{\chi_1 |\Omega|}{4\pi D \mathcal{U}_0} \right] . \tag{4.13 b}$$

In (4.13 b) the Green's matrix $\mathcal{G}$, the capacitance vector $\mathbf{c}$, and the vector $\mathbf{P}_{1p}$ are defined in (3.22), while χ_1 is defined in (3.23 b). The Neumann Green's function G and the function P_{1p} are defined by (3.13) and (3.14), respectively.

We now use this result together with (4.2) to calculate the conditional mean first passage time $\mathbb{T}$ in the outer region. By expanding $\mathbb{T} = \varepsilon^{-1} \mathbb{T}_0 + \mathbb{T}_1 + \cdots$, we obtain from (4.2) that

$$\mathbb{T}_0 = \frac{\mathcal{U}_0}{\mathcal{P}_0} = \frac{|\Omega|}{D\gamma} \,, \qquad \mathbb{T}_1 = -\frac{\mathcal{P}_1 \mathcal{U}_0}{\mathcal{P}_0^2} + \frac{\mathcal{U}_1}{\mathcal{P}_0} \,, \tag{4.14}$$

with $\mathcal{P}_0 = 4\pi c_1 / \gamma$. Upon substituting $\mathcal{P}_j$ and $\mathcal{U}_j$ for $j = 0, 1$ as given in (3.23) and (4.13), respectively, into (4.14), we can identify $\mathbb{T}_1$ after some algebraic manipulations. This leads to one of our main results:

Principal Result 4.2: *In the limit $\varepsilon \to 0$, the conditional MFPT $\mathbb{T}$ satisfying (4.1) is given asymptotically in the outer region $|\mathbf{x} - \mathbf{x}_j| \gg \mathcal{O}(\varepsilon)$ for $j = 1, \ldots, M$ by*

$$\mathbb{T} \sim \frac{\mathbb{T}_0}{\varepsilon} + \mathbb{T}_1 + o(1) = \frac{|\Omega|}{D\gamma\varepsilon} + \left(-\frac{|\Omega|}{D} G(\mathbf{x}; \mathbf{x}_1) + \bar{\mathbb{T}}_1 \right) + o(1) \,. \tag{4.15 a}$$

Here, $\bar{\mathbb{T}}_1$ defined in terms of χ_1 and $\bar{\mu}_1$ of (3.23 b) and (4.13 b), respectively, is given by

$$\bar{\mathbb{T}}_1 \equiv \frac{\bar{\mu}_1}{\mathcal{P}_0} - \frac{\mathcal{U}_0 \chi_1}{\mathcal{P}_0^2} = \frac{4\pi D \mathbb{T}_0^2}{|\Omega|} \left[\mathcal{J}(\mathbf{x}_1, \ldots, \mathbf{x}_M) + \frac{\kappa^2}{4\pi} \int_{\partial\Omega} P_{1p} \, d\mathbf{x} \right] , \qquad \mathcal{J}(\mathbf{x}_1, \ldots, \mathbf{x}_M) \equiv 4\pi \mathbf{c}^T \mathcal{G} \mathbf{c} + 2\kappa \mathbf{c}^T \mathbf{P}_{1p} \,. \tag{4.15 b}$$

We remark that the function $\mathcal{J}(\mathbf{x}_1,\dots,\mathbf{x}_M)$ in (4.15 b) depends on the trap locations, and their associated capacitances, and the boundary sticky parameter κ. In terms of $\mathbb{T}_0$ and $\bar{\mathbb{T}}_1$, the average conditional MFPT, labeled as $\langle\mathbb{T}\rangle$, is given by

$$\langle T\rangle = \frac{\int_\Omega \mathcal{P}\mathbb{T}\,d\mathbf{x}}{\int_\Omega \mathcal{P}\,d\mathbf{x}} = \frac{\int_\Omega \mathcal{U}\,d\mathbf{x}}{\int_\Omega \mathcal{P}\,d\mathbf{x}} \sim \frac{\varepsilon^{-1}\mathcal{U}_0|\Omega| + \bar{\mu}_1|\Omega|}{\mathcal{P}_0|\Omega| + \varepsilon\chi_1|\Omega|} \sim \frac{\mathcal{U}_0}{\varepsilon\mathcal{P}_0} + \left(\frac{\bar{\mu}_1}{\mathcal{P}_0} - \frac{\mathcal{U}_0\chi_1}{\mathcal{P}_0^2}\right) + \cdots = \frac{\mathbb{T}_0}{\varepsilon} + \bar{\mathbb{T}}_1 + \cdots . \tag{4.15 c}$$

To illustrate (4.15), let Ω be a sphere of radius L containing M small spherical traps of radii εa_j centered at $\mathbf{x}_j \in \Omega$ for $j = 1,\dots,M$. Then, we set $c_j = a_j$ in (4.15 b) and use (3.27) for P_{1p}. In this way, (4.15) reduces to

$$\mathbb{T} \sim \frac{\mathbb{T}_0}{\varepsilon} - \frac{4\pi L^3}{3D}G(\mathbf{x};\mathbf{x}_1) + \frac{3D\mathbb{T}_0^2}{L^3}\left[4\pi\mathbf{a}^T\mathcal{G}\mathbf{a} + \frac{\kappa}{L}\sum_{i=1}^{M} a_i|\mathbf{x}_i|^2 - \frac{3\kappa LM\bar{a}}{5} + \frac{\kappa^2L^3}{5}\right] + o(1)\,, \tag{4.16}$$

where $\mathbb{T}_0 = L^3/[3D(L^2\kappa + \bar{a}M)]$ and $\mathbf{a}^T = (a_1,\dots,a_M)$. In (4.16), the Green's matrix $\mathcal{G}$ and $G(\mathbf{x};\mathbf{x}_1)$ can be calculated explicitly from (3.25). For the radially symmetric concentric sphere case, where $\Omega = \{|\mathbf{x}|\,|\,\varepsilon < |\mathbf{x}| < L\}$, we set $M = 1$ and $c_1 = 1$ in (4.16) and use (3.26) for G and R. This yields,

$$\mathbb{T} \sim \frac{L^3}{3D\varepsilon\,(1+\kappa L^2)} + \frac{1}{6D}\left(-r^2 - \frac{2L^3}{r}\right) + \frac{\kappa L^4}{3D\,(1+\kappa L^2)^2}\left(3 + 2\kappa L^2\right) + o(1)\,. \tag{4.17}$$

As a partial validation of (4.15), we show that (4.17) can be recovered from the exact solution for $\mathbb{T}$ given in (2.15 b) for concentric spheres. To do so, we set $a = \varepsilon$ and $\lambda = \varepsilon\kappa$ in (2.15 b), and expand the resulting expression for $\varepsilon \ll 1$ to obtain

$$\begin{aligned}\mathbb{T} &\sim \frac{1}{6D}\left(r(2L-r)\right) - \frac{L}{3Dr}(L-r)^2 + \frac{L}{3D\varepsilon}\frac{\left(L^2 - 2\varepsilon L\right)}{\left[(1+\kappa L^2) - \varepsilon\kappa L\right]}\,,\\ &\sim \frac{L^3}{3D\varepsilon(1+\kappa L^2)} + \frac{1}{6D}\left(-r^2 - \frac{2L^3}{r} + 4L^2\right) + \frac{1}{3D(1+\kappa L^2)}\left(-2L + \frac{\kappa L^3}{1+\kappa L^2}\right)\,.\end{aligned}$$

By re-arranging this last expression we readily obtain (4.17).

Next, we briefly discuss the solution for $\mathbb{T}$ in the inner region near the j-th trap. In the inner region near the non-target traps $j = 2,\dots,M$, we have $\mathcal{U} \sim \varepsilon^{-1}\mu_0 = \varepsilon^{-1}\mathcal{U}_0(1-w_{cj})$ and $\mathcal{P} \sim w_0 = \mathcal{P}_0(1-w_{cj})$ from (3.8). Therefore, we have that $\mathbb{T} \equiv \mathcal{U}/\mathcal{P} \sim \mathcal{U}_0/(\varepsilon\mathcal{P}_0) = \mathbb{T}_0/\varepsilon$ in the inner region near the non-target traps, where $\mathbb{T}_0 = |\Omega|/(D\gamma\varepsilon)$ from (4.15 a). However, near the target trap Ω_{ε_1} we have $\mathcal{U} \sim \varepsilon^{-1}\mu_0 = \varepsilon^{-1}\mathcal{U}_0(1-w_{cj})$ and $\mathcal{P} \sim w_0 = \mathcal{P}_0 + (1-\mathcal{P}_0)w_{cj}$ from (3.8), so that $\mathbb{T} \equiv \varepsilon^{-1}\mathbb{T}_0(1-w_{c1})/(1+(1-P_0)w_{c1}/P_0)$. In particular, if Ω_{ε_1} is a sphere of radius εa_1, then we get in the inner region near the target trap Ω_{ε_1} that

$$\mathbb{T} \sim \frac{\mathbb{T}_0}{\varepsilon}\left[1 - \frac{a_1}{|\mathbf{y}_1|}\right]\left[1 + \left(\frac{1-\mathcal{P}_0}{\mathcal{P}_0}\right)\frac{a_1}{|\mathbf{y}_1|}\right]^{-1}\,, \tag{4.18}$$

where $\mathbb{T}_0$ and $\mathcal{P}_0$ are given in (4.15 a) and (3.12), respectively.

4.1 Conditional Second Moment and Variance

Next, we calculate the conditional second moment $\mathbb{T}_2$ satisfying

$$\Delta\left[\mathcal{P}\mathbb{T}_2\right] = -\frac{2\mathcal{P}\mathbb{T}}{D}\,, \quad \mathbf{x}\in\Omega\backslash\Omega_p\,; \qquad \partial_n\left[\mathcal{P}\mathbb{T}_2\right] + \varepsilon\kappa\left[\mathcal{P}\mathbb{T}_2\right] = 0\,, \quad \mathbf{x}\in\partial\Omega\,, \tag{4.19 a}$$

$$\mathcal{P}\mathbb{T}_2 = 0\,, \quad \mathbf{x}\in\partial\Omega_{\epsilon_1}\,; \qquad \mathcal{P}\mathbb{T}_2 \to 0\,, \quad \mathbf{x}\in\partial\Omega_{\epsilon_j}\,, \quad j = 2,\dots,M\,. \tag{4.19 b}$$

Here $\mathcal{P}$ and $\mathbb{T}$ is the splitting probability and conditional MFPT satisfying (3.1) and (4.1) when $\lambda = \varepsilon\kappa$, which were given asymptotically in Principal Results 3.1 and 4.2, respectively. To analyze (4.19), it is convenient to introduce $\mathcal{V}$ by

$$\mathbb{T}_2 = \mathcal{V}/\mathcal{P}\,. \tag{4.20}$$

Upon recalling that $\mathcal{U} = \mathcal{P}\mathbb{T}$ from (4.2), we get that $\mathcal{V}$ satisfies

$$\Delta\mathcal{V} = -\frac{2\mathcal{U}}{D}\,, \qquad \mathbf{x}\in\Omega\backslash\Omega_p\,; \qquad \partial_n\mathcal{V} + \varepsilon\kappa\mathcal{V} = 0\,, \qquad \mathbf{x}\in\partial\Omega\,, \tag{4.21 a}$$

$$\mathcal{V} = 0\,, \quad \mathbf{x}\in\partial\Omega_{\epsilon_1}\,; \qquad \mathcal{V}\to 0\,, \quad \mathbf{x}\in\partial\Omega_{\epsilon_j}\,, \quad j = 2,\dots,M\,. \tag{4.21 b}$$

We now solve (4.21) by the method of matched asymptotic expansions. Since $\mathcal{U} = \varepsilon^{-1}\mathcal{U}_0 + \mathcal{U}_1 + \cdots$ in the outer region, as given in Principal Result 4.1, we expand $\mathcal{V}$ in the outer region as

$$\mathcal{V} = \varepsilon^{-2}\mathcal{V}_0 + \varepsilon^{-1}\mathcal{V}_1 + \mathcal{V}_2 + \cdots\,, \tag{4.22}$$

where $\mathcal{V}_0$ is an unknown constant. From (4.21 a), we obtain that $\mathcal{V}_k$ for $k = 1, 2$ satisfies

$$\Delta\mathcal{V}_k = -\frac{2\mathcal{U}_{k-1}}{D}\,, \qquad \mathbf{x}\in\Omega\backslash\{\mathbf{x}_1,\dots,\mathbf{x}_M\}\,; \qquad \partial_n\mathcal{V}_k = -\kappa\mathcal{V}_{k-1}\,, \qquad \mathbf{x}\in\partial\Omega\,, \tag{4.23}$$

subject to singularity conditions as $\mathbf{x}\to\mathbf{x}_j$ for $j = 1,\dots,M$ that are to be determined.

In the inner region near the j-th trap, we expand the inner solution $v(\mathbf{y}_j) \equiv \mathcal{V}(\mathbf{x}_j + \varepsilon\mathbf{y}_j)$, with $\mathbf{y}_j \equiv \varepsilon^{-1}(\mathbf{x} - \mathbf{x}_j)$, as

$$v = \varepsilon^{-2}v_0 + \varepsilon^{-1}v_1 + v_2 + \cdots\,. \tag{4.24}$$

Upon substituting (4.24) into (4.21 b) and the PDE of (4.21 a), we obtain that v_k for $k = 0, 1$ satisfies

$$\Delta_y v_k = 0\,, \quad \mathbf{y}_j\notin\Omega_j\,; \qquad v_k = 0\,, \quad \mathbf{y}_j\in\partial\Omega_j\,, \qquad j = 1,\dots,M\,. \tag{4.25}$$

The matching condition between the inner and outer solutions is that for $\mathbf{x}\to\mathbf{x}_j$ and $|\mathbf{y}_j|\to\infty$,

$$\varepsilon^{-2}\mathcal{V}_0 + \varepsilon^{-1}\mathcal{V}_1 + \mathcal{V}_2 + \cdots \sim \varepsilon^{-2}v_0 + \varepsilon^{-1}v_1 + v_2 + \cdots\,. \tag{4.26}$$

The leading order matching condition is that $v_0\to\mathcal{V}_0$ as $|\mathbf{y}_j|\to\infty$. From (4.25), we conclude that $v_0 = \mathcal{V}_0(1 - w_{cj})$, where w_{cj} satisfies (3.9 a). Upon using the far-field behavior of w_{cj} from (3.9 b), we obtain in terms of outer variables that

$$v_0 \sim \mathcal{V}_0\left(1 - \frac{\varepsilon c_j}{|\mathbf{x}-\mathbf{x}_j|} - \frac{\varepsilon^2\mathbf{b}_j\cdot(\mathbf{x}-\mathbf{x}_j)}{|\mathbf{x}-\mathbf{x}_j|^3} + \cdots\right) \qquad \text{as} \quad |\mathbf{y}_j|\to\infty\,. \tag{4.27}$$

Then, from (4.26) we obtain $\mathcal{V}_1 \sim -c_j\mathcal{V}_0/|\mathbf{x}-\mathbf{x}_j|$ as $\mathbf{x}\to\mathbf{x}_j$ for $j = 1,\dots,M$. From (4.23) with $k = 1$, we conclude that

$$\Delta\mathcal{V}_1 = -\frac{2\mathcal{U}_0}{D} + 4\pi\mathcal{V}_0\sum_{i=i}^{M} c_i\delta(\mathbf{x}-\mathbf{x}_i)\,, \qquad \mathbf{x}\in\Omega\,; \qquad \partial_n\mathcal{V}_1 = -\kappa\mathcal{V}_0\,, \qquad \mathbf{x}\in\partial\Omega\,. \tag{4.28}$$

Upon applying the divergence theorem to (4.28), and recalling (4.11) for $\mathcal{U}_0$, we calculate $\mathcal{V}_0$ as

$$\mathcal{V}_0 = \frac{2\mathcal{U}_0|\Omega|}{D\gamma} = \frac{8\pi c_1|\Omega|^2}{D^2\gamma^3}\,, \qquad \gamma \equiv \kappa|\partial\Omega| + 4\pi M\bar{c}\,. \tag{4.29}$$

The solution to (4.28) is written in terms of the Neumann Green's function G of (3.13) and P_{1p} of (3.14), as

$$\mathcal{V}_1(\mathbf{x}) = -4\pi\mathcal{V}_0\sum_{i=1}^{M} c_i G(\mathbf{x};\mathbf{x}_i) - \kappa\mathcal{V}_0 P_{1p}(\mathbf{x}) + \bar{\nu}_1\,, \tag{4.30}$$

where $\bar{\nu}_1 \equiv |\Omega|^{-1}\int_\Omega \mathcal{V}_1\,d\mathbf{x}$ is a constant to be found. The constant $\bar{\nu}_1$ is calculated in Appendix B from a solvability condition on the problem for $\mathcal{V}_2$. In this way, in the outer region the solution $\mathcal{V}$ to (4.21) is given asymptotically by

$$\mathcal{V} \sim \varepsilon^{-2}\mathcal{V}_0 + \varepsilon^{-1}\mathcal{V}_1 + \mathcal{O}(1) = \frac{8\pi c_1|\Omega|^2}{D^2\gamma^3\varepsilon^2} + \varepsilon^{-1}\left(-4\pi\mathcal{V}_0\sum_{i=1}^{M} c_i G(\mathbf{x};\mathbf{x}_i) - \kappa\mathcal{V}_0 P_{1p}(\mathbf{x}) + \bar{\nu}_1\right) + \mathcal{O}(1)\,. \tag{4.31 a}$$

Here γ is defined in (4.29) and $\bar{\nu}_1$ is given in terms of $\bar{\mu}_1$ of (4.13 b) and $\mathcal{J}$ of (4.15 b) as

$$\bar{\nu}_1 = \frac{4\pi\mathcal{V}_0}{\gamma}\left[\mathcal{J}(\mathbf{x}_1,\ldots,\mathbf{x}_M) + \frac{\kappa^2}{4\pi}\int_{\partial\Omega} P_{1p}\,d\mathbf{x} + \frac{\bar{\mu}_1|\Omega|}{2\pi D\mathcal{V}_0}\right]. \tag{4.31 b}$$

We now use (4.31) to calculate the conditional second moment $\mathbb{T}_2$ in the outer region from (4.20). By expanding $\mathbb{T}_2 = \varepsilon^{-2}\mathbb{T}_{20} + \varepsilon^{-1}\mathbb{T}_{21} + \cdots$, we obtain that

$$\mathbb{T}_{20} = \frac{\mathcal{V}_0}{\mathcal{P}_0} = \frac{2|\Omega|^2}{D^2\gamma^2}, \qquad \mathbb{T}_{21} = -\frac{\mathcal{P}_1\mathcal{V}_0}{\mathcal{P}_0^2} + \frac{\mathcal{V}_1}{\mathcal{P}_0}, \tag{4.32}$$

with $\mathcal{P}_0 = 4\pi c_1/\gamma$. Upon substituting $\mathcal{P}_j$ and $\mathcal{V}_j$ for $j = 0, 1$ as given in (3.23 a) and (4.31), respectively, into (4.32), we can identify $\mathbb{T}_{21}$ after a lengthy, but straightforward, calculation. We summarize the result as follows:

Principal Result 4.3: *In the limit $\varepsilon \to 0$, the conditional second moment $\mathbb{T}_2$ satisfying (4.19) is given asymptotically in the outer region $|\mathbf{x} - \mathbf{x}_j| \gg \mathcal{O}(\varepsilon)$ for $j = 1,\ldots,M$ by*

$$\mathbb{T}_2 \sim \varepsilon^{-2}\mathbb{T}_{20} + \varepsilon^{-1}\mathbb{T}_{21} + \mathcal{O}(1) = \frac{2\varepsilon^{-2}|\Omega|^2}{D^2\gamma^2} + \varepsilon^{-1}\left(-\frac{2|\Omega|^2}{D^2\gamma}G(\mathbf{x};\mathbf{x}_1) + \bar{\mathbb{T}}_{2_1}\right) + \mathcal{O}(1). \tag{4.33 a}$$

Here, $\bar{\mathbb{T}}_{2_1}$ defined in terms of χ_1, $\bar{\nu}_1$, and $\mathcal{J}$ in (3.23 b), (4.31 b), and (4.15 b), respectively, is given by

$$\bar{\mathbb{T}}_{2_1} \equiv \frac{\bar{\nu}_1}{\mathcal{P}_0} - \frac{\mathcal{V}_0\chi_1}{\mathcal{P}_0^2} = \frac{16\pi|\Omega|^2}{D^2\gamma^3}\left[\mathcal{J}(\mathbf{x}_1,\ldots,\mathbf{x}_M) + \frac{\kappa^2}{4\pi}\int_{\partial\Omega} P_{1p}\,d\mathbf{x}\right]. \tag{4.33 b}$$

The second moment $\mathbb{T}_2$ can be used to calculate the conditional variance $\mathbb{V}$ defined by $\mathbb{V} = \mathbb{T}_2 - \mathbb{T}^2$. Since $\mathbb{T}_2 = \varepsilon^{-2}\mathbb{T}_{20} + \varepsilon^{-1}\mathbb{T}_{21} + \mathcal{O}(1)$ and $\mathbb{T} = \varepsilon^{-1}\mathbb{T}_0 + \varepsilon^{-1}\mathbb{T}_1 + \mathcal{O}(1)$, we calculate that

$$\mathbb{V} = \mathbb{T}_2 - \mathbb{T}^2 \sim \varepsilon^{-2}\left(\mathbb{T}_{20} - \mathbb{T}_0^2\right) + \varepsilon^{-1}\left(\mathbb{T}_{21} - 2\mathbb{T}_0\mathbb{T}_1\right) + \mathcal{O}(1).$$

Upon using (4.15) and (4.33) for $\mathbb{T}_j$ and $\mathbb{T}_{2j}$, respectively, for $j = 0, 1$, we calculate for $\varepsilon \to 0$ in the outer region that

$$\mathbb{V} \sim \frac{\varepsilon^{-2}|\Omega|^2}{D^2\gamma^2} + \frac{8\pi\varepsilon^{-1}|\Omega|^2}{D^2\gamma^3}\left[\mathcal{J}(\mathbf{x}_1,\ldots,\mathbf{x}_M) + \frac{\kappa^2}{4\pi}\int_{\partial\Omega} P_{1p}\,d\mathbf{x}\right] + \mathcal{O}(1). \tag{4.34}$$

We conclude from (4.34) that the first two terms in the asymptotic expansion of $\mathbb{V}$ are independent of the starting point $\mathbf{x}$ of for the random walk and of the specific target trap. The first term in $\mathbb{V}$ is independent of the locations of the traps, while the second term in $\mathbb{V}$ depends on the trap locations through $\mathcal{J}$. The minimum of $\mathbb{V}$ occurs at the trap configuration that minimizes $\mathcal{J}$. The objective function $\mathcal{J}$ depends on two terms; the inter-trap interaction term $\mathbf{c}^T\mathcal{G}\mathbf{c}$ involving the Green's matrix $\mathcal{G}$, which is minimized when the traps are equi-distributed in the domain, and the boundary interaction term $2\kappa\mathbf{c}^T\mathbf{P}_{1p}$ which is large when either κ is large or when the traps are close to the boundary. In Fig. 5b, for several values of the boundary stickiness parameter κ, we plot $\mathcal{J}$ for the case where 20 small traps are placed at the vertices of a dodecahedron of radius ρ that is concentric with the unit sphere. The locations of the traps for $\rho = 0.7$ are shown in Fig. 5a. As expected, the results show that for each $\kappa > 0$, $\mathcal{J}$ versus ρ has a minimum at some ρ in $0 < \rho < 1$, with the location of this minimum radius decreasing as κ increases.

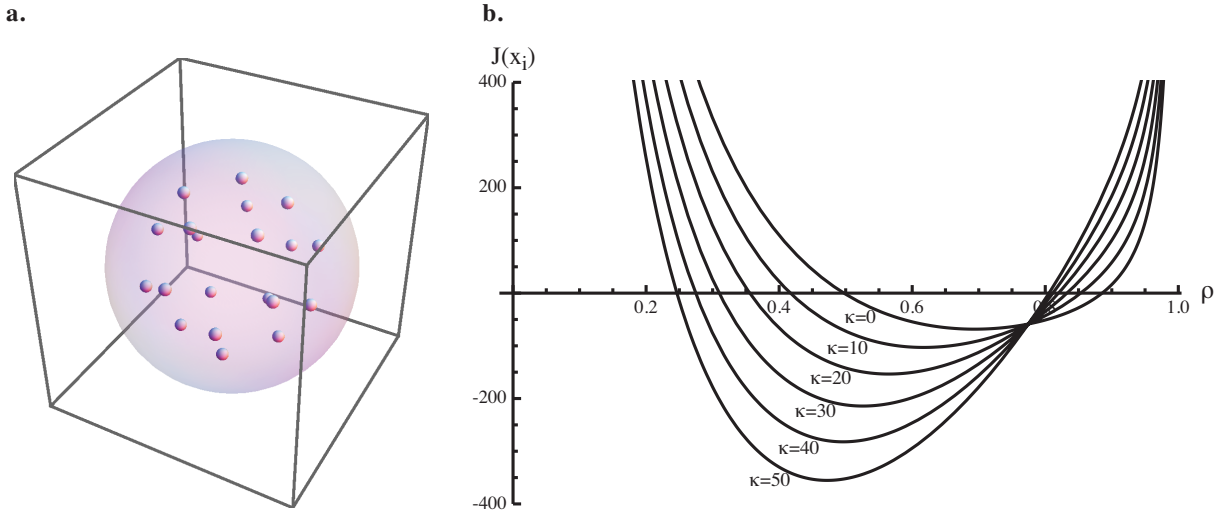

Figure 5. Dodecahedron calculations. Small traps are placed at the vertices of a dodecahedron inscribed on a sphere of radius $0 < \rho < 1$ that lies concentrically within the larger sphere of radius $L = 1$. **a.** The geometry is shown for $\rho = 0.7$. **b.** We plot $\mathcal{J}(\mathbf{x}_1, \ldots, \mathbf{x}_M)$ as a function of the radius of the dodecahedron, for a range of boundary stickiness $\kappa = 0, 10, 20, 30, 40, 50$.

5 Mean First Passage Time, Second Moment, and Variance

In this section we calculate the MFPT, $\mathbb{T}_g$, for a diffusing particle to get captured by any one of a collection of M small traps or on the sticky boundary. This MFPT satisfies

$$\Delta \mathbb{T}_g = -\frac{1}{D}\,, \qquad \mathbf{x} \in \Omega \backslash \Omega_p\,, \tag{5.1 a}$$

$$\partial_n \mathbb{T}_g + \varepsilon\kappa \mathbb{T}_g = 0\,, \quad \mathbf{x} \in \partial\Omega\,; \qquad \mathbb{T}_g = 0\,, \quad \mathbf{x} \in \partial\Omega_{\epsilon_j}\,, \quad j = 1, \ldots, M\,. \tag{5.1 b}$$

We will also calculate the second moment $\mathbb{T}_{g2}$ of this process, which satisfies

$$\Delta \mathbb{T}_{g2} = -\frac{2\mathbb{T}_g}{D}\,, \qquad \mathbf{x} \in \Omega \backslash \Omega_p\,, \tag{5.2 a}$$

$$\partial_n \mathbb{T}_{g2} + \varepsilon\kappa \mathbb{T}_{g2} = 0\,, \quad \mathbf{x} \in \partial\Omega\,; \qquad \mathbb{T}_{g2} = 0\,, \quad \mathbf{x} \in \partial\Omega_{\epsilon_j}\,, \quad j = 1, \ldots, M\,. \tag{5.2 b}$$

To calculate the asymptotics of $\mathbb{T}_g$ expediently, we observe upon comparing (5.1) with (4.3) that $\mathbb{T}_g = \mathcal{U}$ if we simply set $\mathcal{P} = 1$ in (4.3 *a*). Similarly, to calculate $\mathbb{T}_{g2}$, we observe upon comparing (5.2) with (4.21) that $\mathbb{T}_{g2} = \mathcal{V}$ if we simply replace $\mathcal{U}$ in (4.21 *a*) with $\mathbb{T}_g$. In this way, we obtain the following main result for $\mathbb{T}_g$ and $\mathbb{T}_{g2}$:

Principal Result 5.1: *In the limit $\varepsilon \to 0$, the MFPT, $\mathbb{T}_g$, satisfying (5.1) is given asymptotically in the outer region $|\mathbf{x} - \mathbf{x}_j| \gg \mathcal{O}(\varepsilon)$ for $j = 1, \ldots, M$ by*

$$\mathbb{T}_g \sim \frac{\mathbb{T}_{g0}}{\varepsilon} + \mathbb{T}_{g1} + o(1) = \frac{|\Omega|}{D\gamma\varepsilon} + \left(-4\pi \mathbb{T}_{g0} \sum_{i=1}^{M} c_i G(\mathbf{x}; \mathbf{x}_i) - \kappa \mathbb{T}_{g0} P_{1p}(\mathbf{x}) + \bar{\mathbb{T}}_{g_1} \right) + o(1)\,, \tag{5.3 a}$$

where γ is defined in (4.11). Here $\bar{\mathbb{T}}_{g_1}$ is given in terms of $\mathcal{J}$ of (4.15 b) by

$$\bar{\mathbb{T}}_{g_1} = \frac{4\pi \mathbb{T}_{g0}}{\gamma} \left[\mathcal{J}(\mathbf{x}_1, \ldots, \mathbf{x}_M) + \frac{\kappa^2}{4\pi} \int_{\partial\Omega} P_{1p}\, d\mathbf{x} \right]\,. \tag{5.3 b}$$

In addition, for $\varepsilon \to 0$, the second moment $\mathbb{T}_{g2}$ satisfying (5.2) is given asymptotically in the outer region by

$$\mathbb{T}_{g2} \sim \varepsilon^{-2}\mathbb{T}_{g2_0} + \varepsilon^{-1}\mathbb{T}_{g2_1} + \cdots = \frac{2\varepsilon^{-2}|\Omega|^2}{D^2\gamma^2} + \varepsilon^{-1}\left(-4\pi\mathbb{T}_{g2_0}\sum_{i=1}^{M} c_i G(\mathbf{x};\mathbf{x}_i) - \kappa\mathbb{T}_{g2_0}P_{1p}(\mathbf{x}) + \bar{\mathbb{T}}_{g2_1}\right) + \cdots , \tag{5.4 a}$$

where $\bar{\mathbb{T}}_{g2_1}$ is given by

$$\bar{\mathbb{T}}_{g2_1} \equiv \frac{4\pi\mathbb{T}_{g2_0}}{\gamma}\left[\mathcal{J}(\mathbf{x}_1,\ldots,\mathbf{x}_M) + \frac{\kappa^2}{4\pi}\int_{\partial\Omega} P_{1p}\,d\mathbf{x} + \frac{\bar{\mathbb{T}}_{g_1}|\Omega|}{2\pi D\mathbb{T}_{g2_0}}\right] , \tag{5.4 b}$$

A two-term expansion for the variance $\mathbb{V}_g \equiv \mathbb{T}_{g2} - {\mathbb{T}_g}^2$ in the outer region is

$$\mathbb{V}_g \sim \frac{|\Omega|^2\varepsilon^{-2}}{D^2|\gamma|^2} + \frac{8\pi\varepsilon^{-1}|\Omega|^2}{D^2\gamma^3}\left(\mathcal{J}(\mathbf{x}_1,\ldots,\mathbf{x}_M) + \frac{\kappa^2}{4\pi}\int_{\Omega} P_{1p}\,d\mathbf{x}\right) + \mathcal{O}(1)\,. \tag{5.5}$$

We remark that for the special case where $\kappa = 0$, the result (5.3) for $\mathbb{T}_g$ agrees with that obtained in Principal Result 3.1 of [**17**]. Secondly, we observe upon comparing (4.34) and (5.5) that the two term expansions for the variance and the conditional variance are identical. These two expressions, however, differ at the third $\mathcal{O}(1)$ term in their asymptotic expansions. The difficulty with determining this third term explicitly is that we would require an explicit calculation of the third term $\mathcal{U}_2$ and $\mathcal{V}_2$ in the asymptotic expansion of $\mathcal{U}$ and $\mathcal{V}$ in (4.4) and (4.22), respectively. These correction terms satisfy the PDE's of (A.4) and (B.4) in Appendices A and B, respectively.

As a partial validation of (5.3) suppose that Ω is a sphere of radius L that contains exactly one trap of radius ε centered at the origin. For this concentric spherical geometry, the solution to (5.1) is

$$\mathbb{T}_g = -\frac{r^2}{6D} + A\left(\frac{1}{r} - \frac{1}{\varepsilon}\right) + \frac{\varepsilon^2}{6D}\,, \qquad A \equiv -\frac{L^3}{3D}\frac{(1+\varepsilon\kappa L/2)}{[1+\kappa L^2 - \varepsilon\kappa L]}\,. \tag{5.6}$$

For $\varepsilon \to 0$, this exact result reduces to

$$\mathbb{T}_g \sim \frac{L^3}{3D\varepsilon\,(1+\kappa L^2)} - \frac{L^3}{3D\,(1+\kappa L^2)\,r} - \frac{r^2}{6D} + \frac{L^4\kappa\left(3+\kappa L^2\right)}{6D\,(1+\kappa L^2)^2}\,. \tag{5.7}$$

We now compare (5.7) with (5.3). We set $M = 1$, $\mathbf{x}_1 = \mathbf{0}$ in (5.3) and use (3.26) and (3.27) for $G(\mathbf{x};\mathbf{0})$, $R(\mathbf{0})$, and P_{1p}, respectively. Since $P_{1p}(\mathbf{0}) = -3L/10$ and $\int_\Omega P_{1p}\,d\mathbf{x} = 4\pi L^3/5$, (5.3) becomes

$$\mathbb{T}_g \sim \frac{\mathbb{T}_{g_0}}{\varepsilon} + \mathbb{T}_{g_0}\left[-\frac{1}{r} - \frac{r^2}{2L^3} + \frac{9}{5L} - \kappa\left(\frac{r^2}{2L} - \frac{3L}{10}\right) + \frac{1}{1+\kappa L^2}\left(-\frac{9}{5L} - \frac{3\kappa L}{5} + \frac{\kappa^2 L^3}{5}\right)\right] ,$$

where $\mathbb{T}_{g_0} \equiv L^3/\left[3D(1+\kappa L^2)\right]$. By re-arranging this result we recover (5.7). For the special case where $\kappa = 0$, we get

$$\mathbb{T}_g \sim \frac{\mathbb{T}_{g_0}}{\varepsilon} - \frac{\mathbb{T}_{g_0}}{r} - \frac{r^2}{6D}\,, \qquad \mathbb{T}_{g_0} \equiv \frac{L^3}{3D}\,. \tag{5.8}$$

For this concentric spherical geometry, and with $\kappa = 0$, the variance from (5.5) is

$$\mathbb{V}_g \sim \frac{L^6}{9D^2\varepsilon^2} - \frac{2L^5}{5D^2\varepsilon} + \mathcal{O}(1)\,. \tag{5.9}$$

The results (5.8) and (5.9) are in agreement with a two-term expansion of the exact results for $\mathbb{T}_g$ and $\mathbb{V}_g$ as given by setting $a = \varepsilon$ in (2.3 *a*) and (2.4 *a*), respectively.

Finally, we calculate the MFPT, T, to a specific cognate APC, Ω_{ε_1}, when the T cell is unable to leave the lymph node and the T cell keeps its search after contacting irrelevant APCs. This is effectively done by imposing a Neumann boundary condition on the boundary $\partial\Omega$ and on all other targets ($j = 2,\ldots,M$). Under this model, a contact between the T cell

and a non-cognate APC is infinitesimally short. The PDE to be solved for T is

$$\Delta T = -\frac{1}{D}\,, \qquad \mathbf{x}\in\Omega\backslash\Omega_p\,; \qquad \partial_n T = 0\,, \quad \mathbf{x}\in\partial\Omega\,, \tag{5.10 a}$$

$$T = 0\,, \quad \mathbf{x}\in\partial\Omega_{\epsilon_1}\,; \qquad \partial_n T = 0\,, \quad \mathbf{x}\in\partial\Omega_{\varepsilon_j}\,, \quad j=2,\ldots,M\,. \tag{5.10 b}$$

Since the matched asymptotic expansion analysis needed to solve (5.10) for $\varepsilon\to 0$ is similar to that already performed for the other problems we simply give the main result.

Principal Result 5.2: *In the limit $\varepsilon\to 0$, the MFPT, T, satisfying (5.10) is given asymptotically in the outer region $|\mathbf{x}-\mathbf{x}_j|\gg\mathcal{O}(\varepsilon)$ for $j=1,\ldots,M$ by*

$$T\sim\frac{T_0}{\varepsilon}+\frac{|\Omega|}{D}\left[R(\mathbf{x}_1)-G(\mathbf{x};\mathbf{x}_1)\right]+\cdots\,, \tag{5.11}$$

where $T_0=|\Omega|/(4\pi D c_1)$ while $G(\mathbf{x};\mathbf{x}_1)$ and $R(\mathbf{x}_1)$ are the Green's function and its regular part satisfying (3.13). In the inner region near the target trap Ω_{ε_1} we have

$$T\sim\frac{T_0}{\varepsilon}\left(1-w_{c_1}\right)+\mathcal{O}(\varepsilon)\,.$$

where w_{c_1} satisfies (3.9 a) with $j=1$. In contrast, in the inner region near the non-target traps Ω_{ε_j} for $j=2,\ldots,M$, we have that $\mathbb{T}$ is asymptotically spatially constant and is given by

$$T\sim\frac{T_0}{\varepsilon}+4\pi c_1 T_0\left[R(\mathbf{x}_1)-G(\mathbf{x}_j;\mathbf{x}_i)\right]+\mathcal{O}(\varepsilon)\,.$$

6 Application to T cell search within a lymph node and directions for further study

We now demonstrate how to apply the asymptotic results to the motivating question. Consider a spherical region of radius $L=0.5$mm, containing target antigen-presenting-cells (APC). The measured radius of a typical APC is around 7-15μm but we will treat this as an underestimate of the effective interaction volume due to the finite size of the T cell (which we treat as a point particle) and the diffuse, dendritic structure of typical APCs. Therefore, we will represent each APC as a spherical trap with effective radius on the order of 20μm. To potentially improve on this in the future, it would be useful to know the effective capacitance (c_i in Eq. (3.9 b)) of a complicated structure such as a dendritic cell. It is not analytically possible to determine the capacitance of an arbitrary 3-D object (see Appendix C).

Although the 3-D shape of the target, and its associated capacitance, are not well known, in contrast it is known that the searching T cell has a fairly compact shape, with a characteristic radius of around 3μm. Based on previous theoretical work analyzing two-photon microscopy, we estimate the large-scale effective diffusivity of T cells to be $60\mu\text{m}^2/\text{min}$ [**22**]. To estimate the boundary trapping parameter λ, we calculated the MFPT for a T cell to escape, averaging over all possible starting positions, as $\bar{T}_{\text{esc}}=L(5+\lambda L)/(15D\lambda)$. We then set this averaged MFPT equal to a reasonable estimate of the time of residence for a T cell in a lymph node, 720 minutes [**30**], to obtain the approximation $\lambda\simeq .01/\mu$m and so we estimate $\kappa=4/\mu$m (from Eq. 3.2). Since there is a degree of uncertainty in all these parameters, we present representative results over parameter ranges around these baselines. In Fig. 6a we show the probability of reaching a unique APC before exiting through the boundary. We can see that even for fairly leaky boundaries, there is still a reasonable chance of the T cell finding the APC, and this probability is not particularly sensitive to the starting position. The conditional time taken for the T cell to find the APC is typically hundreds of hours (panels b and c). This time scale is unsurprising: the characteristic time for the T cell to explore the lymph node is roughly $L^2/D=70$ hours, while the volume fraction of the lymph node taken by a single APC is only $(20\mu\text{m}/500\mu\text{m})^3=6.4\times10^{-5}$. Perhaps counterintuitively, the conditional

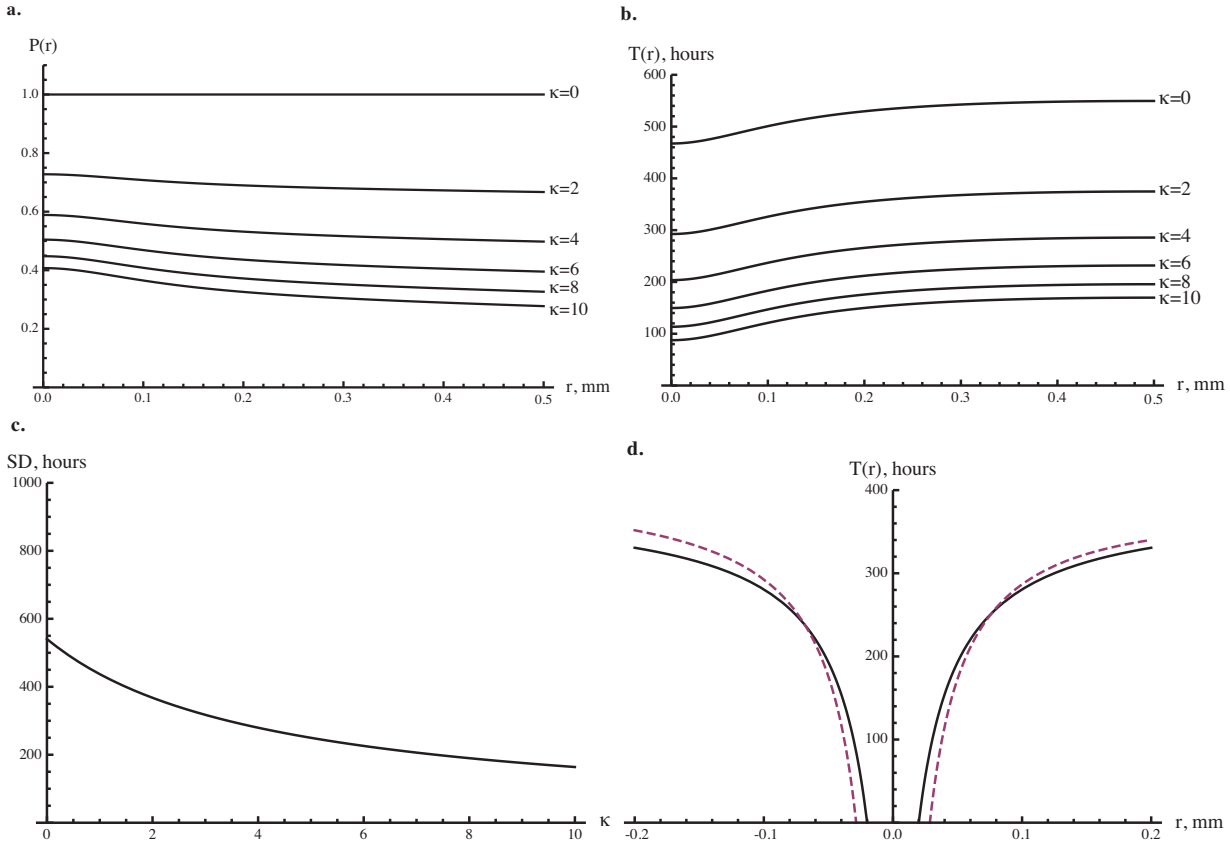

Figure 6. Splitting probability and conditional MFPT for a single target situation. A single target of radius 20μm is located on the z–axis at $(0, 0, 100\mu\text{m})$ and the start point for the searching T cell is taken along the x–axis. **a.** The outer approximation for the splitting probability to reach the target is plotted against the start coordinate for $\kappa = 0, 2, 4, 6, 8, 10/\mu$m. **b.** The corresponding conditional MFPT (outer expansion, Eq. (4.16)) is plotted against the start coordinate for $\kappa = 0, 2, 4, 6, 8, 10/\mu$m. **c.** The first two terms of the expansion for the standard deviation (which are independent of starting position, Eq. (4.34)) are plotted against κ. **d.** The inner (Eq. (4.18), solid line) and outer (Eq. (4.16), dashed line) expansions for the conditional MFPT are plotted around the single target.

capture time decreases with increasing boundary stickiness. This effect is observed because if the boundary is sticky, the T cell must find the APC fairly quickly if it is not to be absorbed at the boundary first.

Our results also extend to scenarios where there are multiple APCs, and with reduced capture times. In Fig. 7, we consider a scenario of T cell search for a single target located near the centre of the spherical lymph node, but this time among either 9 or 24 other randomly located (non-overlapping) competing APCs. We observe (Fig. 7ac) that the probability of reaching the target before any of the competitors declines as the start position of the T cell is moved further away from the target. This effect increases as the permeability (κ) of the boundary is increased. When the start point is far from the target, the splitting probability should on average be close to the location-independent leading-order approximation to Equation 3.23 a (dashed lines). However, in Fig. 7a this is not the case. This is because, in this particular realization of placing the random competing targets, the locations are on average far from the positive x-axis, which is the range of starting positions we show in this figure. In Fig. 7c we are presenting a result with 24 randomly located competing targets, which brings the splitting probability for distant starting points close to the leading-order result in this realization at least. Numerical experiments with many realizations confirm this reasoning (results not shown).

In Fig. 7bd, we show outer approximations (Equation 4.16) to the conditional MFPT to reach the target. We observe

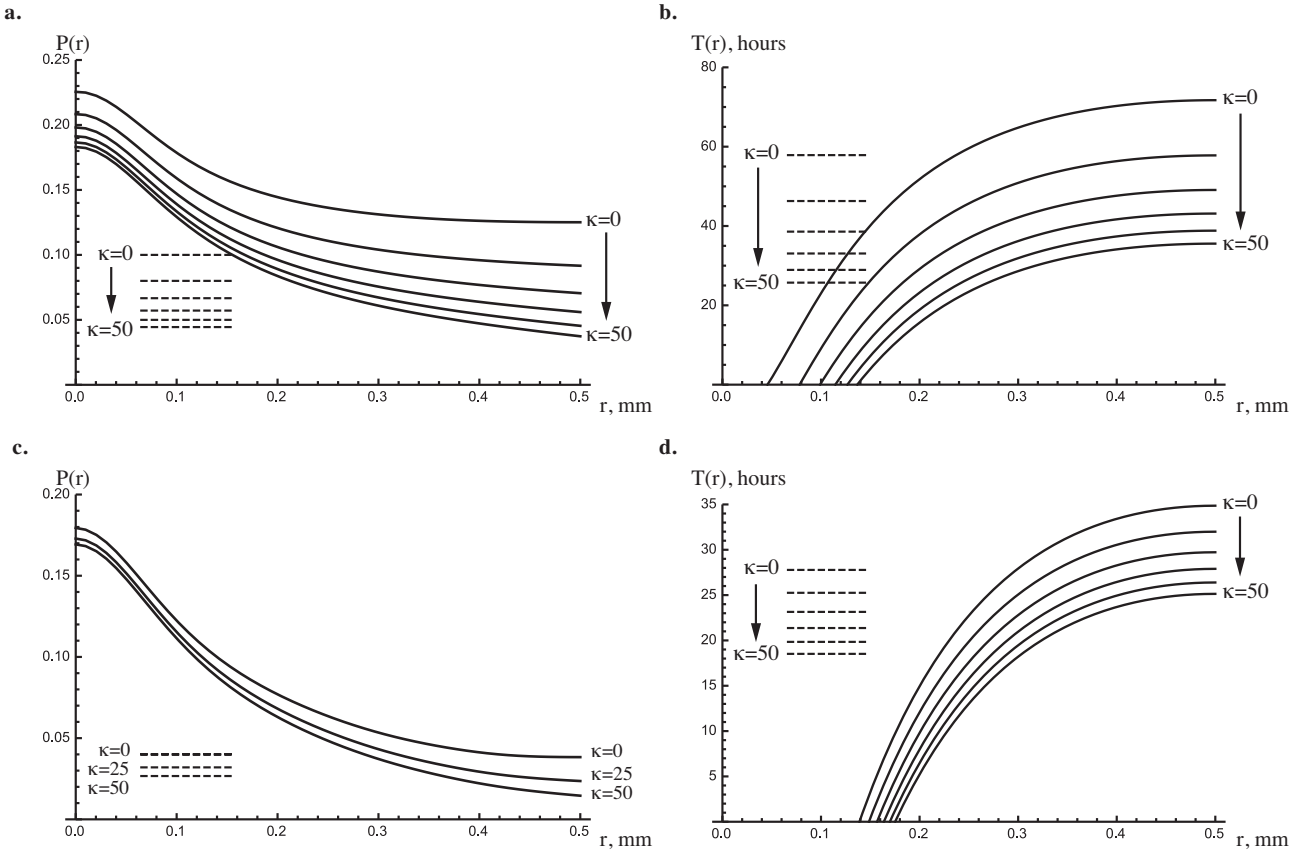

Figure 7. Splitting probability and conditional MFPT to a single target among multiple competing targets.
a. and **c.** Solid lines: The outer approximation (eq. 3.23 *a*) for the splitting probability $\mathcal{P}(r)$ to reach a spherical target centred at position $(0, 0, 0.1\text{mm})$ is plotted over a range of possible start coordinates $(0, 0, r)$, in the presence of (panel **a.**) $M = 9$ and (panel **c.**) $M = 24$ identical competing targets centred at random locations. This calculation was repeated for Neumann ($\kappa = 0$) and Robin boundary conditions with $\kappa = 10, 20, 30, 40, 50$ (panel **a.**) and $\kappa = 25, 50$ (panel **c.**). Dashed lines in **a.** and **c.** indicate the leading order ($\epsilon \to 0$) calculation of $\mathcal{P}(r)$, which is independent of starting position, over the same ranges of κ.
b. and **d.** The outer approximation for the conditional MFPT to the target was calculated (eq. 4.16) using the same geometry as panels **a.** and **c.**, respectively, and using Neumann and Robin boundary conditions as in panel **a.** The dashed lines indicate the leading order ($\epsilon \to 0$) calculation of $T(r)$, which is independent of starting position, over the same range of κ. Parameters: $D = 50 \times 10^{-6}\text{mm}^2/\text{min}$, target radius $\epsilon = 0.02\text{mm}$, outer radius $L = 0.5\text{mm}$.

that the outer approximation is not valid for starting points that are too close to the target (small r values in this plot). This is simply a result of using only the outer expansion in the plot, where this approximation becomes invalid at $\mathcal{O}(\varepsilon)$ distances from a target. Although it is in principle possible to write a composite expansion involving both the outer and inner solutions to eliminate this behavior, such a complication to the analysis is largely unnecessary in most of the domain. We also plot the spatially-independent leading order approximation to the conditional MFPT (dashed lines) which can be interpreted as the conditional MFPT averaged over all possible start positions and target locations.

In Fig. 8, we examine the dependence of the first passage time to *any* of 20 targets on their spatial positions, for a T cell starting position at the origin and a Neumann (reflecting) outer boundary condition. We considered two scenarios. First, we placed the targets randomly (but not overlapping) in a hollow region of the lymph node that excluded the origin (in spherical coordinates, $0.1 < r < 0.5 = L$). A histogram of the MFPT, calculated from 5000 realizations of the

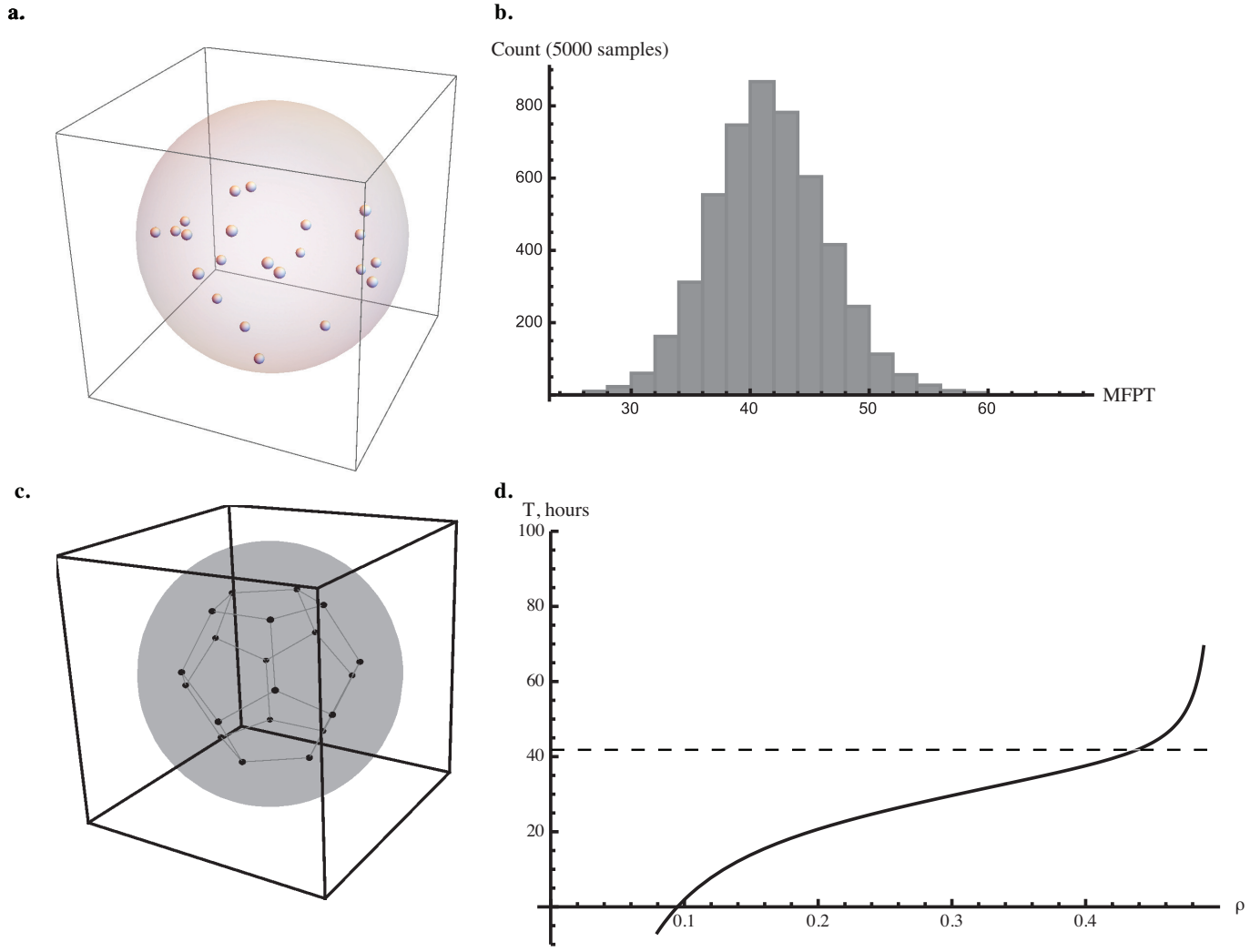

Figure 8. Influence of target distribution on conditional MFPT. **a.** Example of 20 randomly located targets. **b.** Histogram of MFPT to reach *any* of 20 randomly located non-overlapping targets from a centre starting position generated from 5000 realizations of the target configuration, with a Neumann outer boundary condition. (Eq. 5.3 a is used). **c.** The 20 targets are now arranged onto the vertices of a regular dodecahedron. **d.** Conditional MFPT to reach *any* of the organized targets is plotted against the radius ρ of the dodecahedron. The mean of the random configuration (panel **b.**) is indicated with a dashed line. $D = 50 \times 10^{-6}\text{mm}^2/\text{min}$, target radius is $\epsilon = 0.02$mm, outer radius 0.5mm.

target placements is plotted as Fig. 8b. The mean of this plot (41.6h) is higher than the spatially-independent leading order approximation to the MFPT (calculated to be 34.7h from equation 5.3 a) since we enforce that no targets are closer than 0.1 from the start point. We emphasize that the variation in the histogram of MFPT is due to the randomly chosen positions of the 20 targets. Next, we placed the targets on the vertices of a regular dodecahedron of radius ρ. The computed MFPT to any of the regularly spaced targets is plotted as Fig. 8c. This plot is valid away from $\rho = 0$ and $\rho = L = 0.5$. For small radii, the targets are so close to the start point that we are outside the range of validity of the asymptotics. Similarly, the targets must be located away from the outer boundary. However, for intermediate radii of the dodecahedron, we can see that the mean first passage time is significantly less than the average for 20 randomly located targets (41.6 hours, dashed line). This result indicates that careful spatial organization of the target locations could lead to a large reduction of the mean first passage time.

Overall, we feel that our results highlight several important facets of the biological situation. First, under purely diffusive random motion, the time to encounter between a single T cell and a single target antigen-presenting-cell (APC) would be very long, and also improbable if the T cell also has some probability of leaving the lymph node when it reaches the boundary. These findings highlight the importance of having multiple targets present in the lymph node, to increase the likelihood and decrease the delay of a potential immune response. Having multiple targets present could be especially important for small vertebrates such as frogs or mice, that may have a very limited pool of naive T cells bearing a particular antigen specificity. Secondly, as shown in Fig. 8, the spatial organization of the targets can significantly reduce the time to first encounter. Although APC are unlikely to form a dodecahedral net, there would be similar benefits to ensuring that targets are spaced out within the lymph node. This also speaks to an important point of previous studies: that T cell motion is mostly restricted to following the fibroblastic reticular network [**23**, **22**, **24**]. Previous work has shown that T cells approximately follow Brownian motion over sufficiently long time scales [**22**]. However, it is likely that the local behaviour of T cells close to APCs is rather different than pure diffusive and this is a point that we intend to take up in future work.

A final open question for further work is to extend our matched asymptotic approach to a model where the diffusing particle pauses when it reaches an irrelevant (non-target) target. This arises naturally in the context of T cell search, since a T cell would generally pause to closely examine each APC it encounters, searching for known antigens. The T cell in question would remain attached only for a short time and then it would continue its search in the LN. A model of this process in a spherically-shaped domain where the diffusing particle can become intermittently bound to a single trap on the surface has been presented in [**6**] and an extension to multiple surface traps is given in [**38**].

Acknowledgements

We thank Alejandra Herrera and Grant Lythe for useful discussions. MID acknowledges support from the Consejo Naiconal de Ciencia y Tecnología of Mexico (CONACYT) and the Pacific Institute for Mathematical Sciences International Graduate Training Centre in Mathematical Biology. DC and MJW acknowledge grant support from NSERC (Canada).

Appendix A The Conditional MFPT: Calculation of $\bar{\mu}_1$

In this appendix we derive (4.13 *b*) for $\bar{\mu}_1$ of Principal Result 4.1. To do so, we expand the solution $\mathcal{U}_1$ to (4.12) as $\mathbf{x} \to \mathbf{x}_j$, and label $R_j \equiv R(\mathbf{x}_j)$ and $G_{ji} \equiv G(\mathbf{x}_j;\mathbf{x}_i)$. This yields that

$$\mathcal{U}_1 \sim -\frac{c_j \mathcal{U}_0}{|\mathbf{x}-\mathbf{x}_j|} + \mathcal{U}_{1j} + \bar{\mu}_1 + \cdots, \quad \text{as} \quad \mathbf{x} \to \mathbf{x}_j\,; \qquad \mathcal{U}_{1j} \equiv -\kappa \mathcal{U}_0 P_{1p}(\mathbf{x}_j) - 4\pi \mathcal{U}_0 c_j R_j - 4\pi \mathcal{U}_0 \sum_{\substack{i=1 \\ i\neq j}}^{M} c_i G_{ji}\,. \tag{A.1}$$

Upon substituting (A.1) into the matching condition (4.8), we conclude that $u_1 \sim \mathcal{U}_{1j} + \bar{\mu}_1$ as $|\mathbf{y}_j| \to \infty$. The solution to (4.7) with $k = 1$ with this far-field behavior is

$$u_1 = (\mathcal{U}_{1j} + \bar{\mu}_1)\,(1 - w_{cj})\,, \tag{A.2}$$

where w_{cj} satisfies (3.9 *a*). Upon using the far-field behavior (3.9 *b*), we calculate in terms of outer variables that

$$u_1 \sim (\mathcal{U}_{1j} + \bar{\mu}_1)\left(1 - \frac{\varepsilon c_j}{|\mathbf{x}-\mathbf{x}_j|} + \cdots\right), \quad \text{as} \quad |\mathbf{y}_j| \to \infty\,. \tag{A.3}$$

Then, upon substituting (A.3) and (4.9) into the matching condition (4.8), we obtain that $\mathcal{U}_2$ satisfies (4.5) with $k = 2$

subject to the singularity behavior

$$\mathcal{U}_2 \sim -\mathcal{U}_0 \frac{\mathbf{b}_j\cdot(\mathbf{x}-\mathbf{x}_j)}{|\mathbf{x}-\mathbf{x}_j|^3} - (\mathcal{U}_{1j}+\bar{\mu}_1)\,\frac{c_j}{|\mathbf{x}-\mathbf{x}_j|}\,, \qquad \text{as} \quad \mathbf{x}\to\mathbf{x}_j\,.$$

This problem for $\mathcal{U}_2$ is equivalent to

$$\Delta\mathcal{U}_2 = -\frac{P_1}{D} + 4\pi\sum_{i=1}^{M}\left[c_i\,(\mathcal{U}_{1i}+\bar{\mu}_1)\;\delta(\mathbf{x}-\mathbf{x}_i) - \mathcal{U}_0\mathbf{b}_i\cdot\nabla_{\mathbf{x}}\delta(\mathbf{x}-\mathbf{x}_i)\right]\,, \quad \mathbf{x}\in\Omega\,; \qquad \partial_n\mathcal{U}_2 = -\kappa\mathcal{U}_1\,, \quad \mathbf{x}\in\partial\Omega\,. \tag{A.4}$$

From the divergence theorem, and by using $\int_\Omega P_1\,d\mathbf{x} = \chi_1|\Omega|$ from (3.23 a), we obtain that

$$-\frac{\chi_1|\Omega|}{D} + 4\pi\bar{\mu}_1 M\bar{c} + 4\pi\sum_{i=1}^{M} c_i\mathcal{U}_{1i} = -\kappa\int_{\partial\Omega}\mathcal{U}_1\,d\mathbf{x}\,. \tag{A.5}$$

Upon substituting (4.12) for $\mathcal{U}_1$ into the right-hand side of (A.5), we solve for $\bar{\mu}_1$ to get

$$\bar{\mu}_1 = \frac{4\pi}{\gamma}\left[-\sum_{i=1}^{M}\mathcal{U}_{1i}c_i + \frac{\chi_1|\Omega|}{4\pi D} + \kappa\mathcal{U}_0\sum_{i=1}^{M}c_i\int_{\partial\Omega}G(\mathbf{x};\mathbf{x}_i)\,d\mathbf{x} + \frac{\kappa^2\mathcal{U}_0}{4\pi}\int_{\partial\Omega}P_{1p}\,d\mathbf{x}\right]\,. \tag{A.6}$$

Finally, we simplify (A.6) by identifying that $P_{1p}(\mathbf{x}_i) = \int_{\partial\Omega}G(\mathbf{x};\mathbf{x}_i)\,d\mathbf{x}$ from (3.15) and by using (A.1) for $\mathcal{U}_{1i}$. After a short calculation, we obtain (4.13 b) of Principal Result 4.1.

Appendix B The Second Moment for the Conditional MFPT: Calculation of $\bar{\nu}_1$

We outline the derivation of (4.31 b) for $\bar{\nu}_1$. We expand the solution $\mathcal{V}_1$ to (4.30) as $\mathbf{x}\to\mathbf{x}_j$ to obtain

$$\mathcal{V}_1 \sim -\frac{c_j\mathcal{V}_0}{|\mathbf{x}-\mathbf{x}_j|} + \mathcal{V}_{1j} + \bar{\nu}_1 + \cdots\,, \quad \text{as} \quad \mathbf{x}\to\mathbf{x}_j\,; \qquad \mathcal{V}_{1j} \equiv -\kappa\mathcal{V}_0 P_{1p}(\mathbf{x}_j) - 4\pi\mathcal{V}_0 c_j R_j - 4\pi\mathcal{V}_0\sum_{\substack{i=1\\ i\neq j}}^{M} c_i G_{ji}\,. \tag{B.1}$$

Upon substituting (B.1) into the matching condition (4.26), we conclude that $v_1 \sim \mathcal{V}_{1j} + \bar{\nu}_1$ as $|\mathbf{y}_j|\to\infty$. The solution to (4.25) with $k=1$ with this far-field behavior is

$$v_1 = (\mathcal{V}_{1j}+\bar{\nu}_1)\,(1-w_{cj})\,, \tag{B.2}$$

where w_{cj} satisfies (3.9 a). Upon using the far-field behavior (3.9 b), we calculate that

$$v_1 \sim (\mathcal{V}_{1j}+\bar{\nu}_1)\left(1 - \frac{\varepsilon c_j}{|\mathbf{x}-\mathbf{x}_j|} + \cdots\right)\,, \quad \text{as} \quad |\mathbf{y}_j|\to\infty\,. \tag{B.3}$$

Then, upon substituting (B.3) and (4.27) into the matching condition (4.26), we obtain that $\mathcal{V}_2$ satisfies (4.23) with $k=2$ subject to the singularity behavior

$$\mathcal{V}_2 \sim -\mathcal{V}_0\frac{\mathbf{b}_j\cdot(\mathbf{x}-\mathbf{x}_j)}{|\mathbf{x}-\mathbf{x}_j|^3} - (\mathcal{V}_{1j}+\bar{\nu}_1)\,\frac{c_j}{|\mathbf{x}-\mathbf{x}_j|}\,, \quad \text{as} \quad \mathbf{x}\to\mathbf{x}_j\,.$$

This problem for $\mathcal{V}_2$ is equivalent to

$$\Delta\mathcal{V}_2 = -\frac{2\mathcal{U}_1}{D} + 4\pi\sum_{i=1}^{M}\left[c_i\,(\mathcal{V}_{1i}+\bar{\nu}_1)\;\delta(\mathbf{x}-\mathbf{x}_i) - \mathcal{V}_0\mathbf{b}_i\cdot\nabla_{\mathbf{x}}\delta(\mathbf{x}-\mathbf{x}_i)\right]\,, \quad \mathbf{x}\in\Omega\,; \qquad \partial_n\mathcal{V}_2 = -\kappa\mathcal{V}_1\,, \quad \mathbf{x}\in\partial\Omega\,. \tag{B.4}$$

From the divergence theorem, and by using $\int_\Omega\mathcal{U}_1\,d\mathbf{x} = \bar{\mu}_1|\Omega|$ from (4.12), we obtain that

$$-\frac{2\bar{\mu}_1|\Omega|}{D} + 4\pi\bar{\nu}_1 M\bar{c} + 4\pi\sum_{i=1}^{M}c_i\mathcal{V}_{1i} = -\kappa\int_{\partial\Omega}\mathcal{V}_1\,d\mathbf{x}\,. \tag{B.5}$$

Upon substituting (4.30) for $\mathcal{V}_1$ into the right-hand side of (B.5), we get

$$-\frac{2\bar{\mu}_1|\Omega|}{D}+4\pi\bar{\nu}_1 M\bar{c}+4\pi\sum_{i=1}^{M}c_i\mathcal{V}_{1i}=4\pi\kappa\mathcal{V}_0\sum_{i=1}^{M}c_iP_{1p}(\mathbf{x}_i)+\kappa^2\mathcal{V}_0\int_{\partial\Omega}P_{1p}\,d\mathbf{x}-\kappa|\partial\Omega|\bar{\nu}_1\,. \tag{B.6}$$

Finally, we substitute (B.1) for $\mathcal{V}_{1i}$ into (B.6) and then solve the resulting expression for $\bar{\nu}_1$. This yields (4.31 *b*).

Appendix C On the capacitance of an arbitrarily shaped cell

Our asymptotic formulae could be made more accurate using information about the effective capacitance (c_i in Eq. (3.9 *b*)) of a complicated cell structure such as a dendritic cell. A table of formulae for the capacitances of a few simple objects other than a sphere is given in Table 1 of [**17**]. A key rigorous result is that of all compact objects of the same volume the sphere has the smallest capacitance (cf. [**44**]). Therefore, the capacitance of a complicated spiny object such as a dendritic cell is likely much larger than that of a sphere with the same volume. However, to determine an exact value for this capacitance a boundary integral numerical method would have to be employed. With such a larger more biologically realistic estimate of the capacitance than we used below, it follows since our asymptotic analysis involves the product εc_i, that the time-scales reported below in our numerical computations would likely be reduced by a non-negligible factor. As a crude estimate of this factor, consider the well-known capacitance of two identical separated spheres having a common radius εa_c with $a_c=1/2^{1/3}$ and a center-to-center distance εd_c with $d_c>2a_c$. The volume of this two-sphere cluster is $4\pi\varepsilon^3/3$, i.e. it is that of an equivalent sphere of radius ε, and its capacitance c_c as defined in (3.9 *b*) is (cf. [**43**])

$$c_c=\frac{a_c}{2}\sinh(\beta)\sum_{n=1}^{\infty}\frac{1}{\sinh(n\beta)}\,,\qquad\text{where}\quad\cosh(\beta)\equiv\frac{d_c}{2a_c}\,.$$

In the limit for which the two spheres are almost touching, for which $d_c\to 2a_c$ from above, we have

$$c_c\sim\frac{a_c}{2}\left[-\frac{1}{2}\log\left(\frac{d_c}{a_c}-2\right)+\gamma_e+\log 2+o(1)\right]\,,\qquad a_c=1/2^{1/3}\,, \tag{C.1}$$

where $\gamma_e\approx 0.577216$ is Euler's constant. Taking $d_c=2.005a_c$, (C.1) yields $c_c\approx 1.555$, which is roughly a 55% increase over using the capacitance $c=1$ of the equivalent sphere.

References

[1] H. Ammari, J. Garnier, H. Kang, H. Lee, and K. Solna, *The mean escape time for a narrow escape problem with multiple switching gates*, SIAM Multiscale Modeling and Simulation, 9 (2011), pp. 817–833.

[2] M. Bajénoff, N. Glaichenhaus, and R. N. Germain, *Fibroblastic reticular cells guide T lymphocyte entry into and migration within the splenic T cell zone*, J Immunol, 181 (2008), pp. 3947–54.

[3] C. Beauchemin, N. M. Dixit, and A. S. Perelson, *Characterizing T cell movement within lymph nodes in the absence of antigen*, J Immunol, 178 (2007), pp. 5505–12.

[4] J. B. Beltman, A. F. M. Marée, and R. J. de Boer, *Spatial modelling of brief and long interactions between T cells and dendritic cells*, Immunol Cell Biol, 85 (2007), pp. 306–14.

[5] J. B. Beltman, A. F. M. Marée, J. N. Lynch, M. J. Miller, and R. J. de Boer, *Lymph node topology dictates T cell migration behavior*, J Exp Med, 204 (2007), pp. 771–80.

[6] O. Benichou, D. S. Grebenkov, P. E. Levitz, C. Loverdo, and R. Voituriez, *Mean first-passage time of surface-mediated diffusion in spherical domains*, J. Stat. Phys., 142 (2011), pp. 657–685.

[7] O. Benichou and R. Voituriez, *From first-passage times of random walks in confinement to geometry-controlled kinetics*, Physics Reports, 539 (2014), pp. 225–284.

[8] H. C. Berg and E. M. Purcell, *Physics of chemoreception*, Biophys J, 20 (1977), pp. 193–219.

[9] G. Bogle and P. R. Dunbar, *Simulating T-cell motility in the lymph node paracortex with a packed lattice geometry*, Immunol Cell Biol, 86 (2008), pp. 676–87.

[10] P. C. Bressloff and J. Newby, *Stochastic models of intracellular transport*, Rev. Mod. Physics, 85 (2013), pp. 135–196.

[11] M. D. Cahalan, I. Parker, S. H. Wei, and M. J. Miller, *Real-time imaging of lymphocytes in vivo*, Curr Opin Immunol, 15 (2003), pp. 372–7.
[12] D. M. Catron, A. A. Itano, K. A. Pape, D. L. Mueller, and M. K. Jenkins, *Visualizing the first 50 hr of the primary immune response to a soluble antigen*, Immunity, 21 (2004), pp. 341–7.
[13] S.a Celli, M. Day, A. J. Müller, C. Molina-Paris, and G. Lythe, *How many dendritic cells are required to initiate a t-cell response?*, Blood, 120 (2012), pp. 3945–3948.
[14] X. Chen and A. Friedman, *Asymptotic analysis for the narrow escape problem*, SIAM J. Math. Anal., 43 (2011), pp. 2542–2563.
[15] C. Chevalier, O. Bénichou, B. Meyer, and R. Voituriez, *First-passage quantities of Brownian motion in a bounded domain with multiple targets: a unified approach*, Journal of Physics A, Mathematical and Theoretical, 44 (2011).
[16] A. Cheviakov, M. J. Ward, and R. Straube, *An asymptotic analysis of the mean first passage time for narrow escape problems: Part II: the sphere*, SIAM Multiscale Modeling and Simulation, 8 (2010), pp. 836–870.
[17] A. F. Cheviakov and M. J. Ward, *Optimizing the principal eigenvalue of the laplacian in a sphere with interior traps*, Math. Comp. Modeling, 53 (2010), p. 042118.
[18] A. F. Cheviakov and D. Zawada, *Narrow escape problem for the unit sphere: Homogenization limit, optimal arrangements of large numbers of traps, and the n^2 conjecture*, Phys. Rev. E, 87 (2013).
[19] Frank C. Collins and George E. Kimball, *Diffusion-controlled reaction rates*, J. Coll. Sci., 4 (1949), pp. 425–437.
[20] M. Day and G. Lythe, *Timescales of the adaptive immune response*, Mathematical Models and Immune Cell Biology, (2011), pp. 351–361.
[21] M. S. Day, *Stochastic Modelling of Lymphocyte Dynamics and Interactions*, PhD thesis, University of Leeds, 2013.
[22] G. M. Donovan and G. Lythe, *T-cell movement on the reticular network*, J Theor Biol, 295 (2012), pp. 59–67.
[23] F. Graw and R. R. Regoes, *Investigating CTL mediated killing with a 3D cellular automaton*, PLoS Comput Biol, 5 (2009), p. e1000466.
[24] ———, *Influence of the fibroblastic reticular network on cell-cell interactions in lymphoid organs*, PLoS Comput Biol, 8 (2012), p. e1002436.
[25] I. L. Grigorova, M. Panteleev, and J. G. Cyster, *Lymph node cortical sinus organization and relationship to lymphocyte egress dynamics and antigen exposure*, Proc Natl Acad Sci U S A, 107 (2010), pp. 20447–52.
[26] D. Holcman, A. Marchewka, and Z. Schuss, *Survival probability of diffusion with trapping in cellular neurobiology*, Phys Rev E, 72 (2005), p. 031910.
[27] D. Holcman and Z. Schuss, *The narrow escape problem*, SIAM Review, 56 (2014), pp. 213–257.
[28] J.D. Jackson, *Classical Electrodynamics*, Wiley, New York, 1945.
[29] S. Karlin and H. M. Taylor, *A Second Course in Stochastic Processes*, Academic Press, San Diego, 1981.
[30] J. N. Mandl, R. Liou, F. Klauschen, N. Vrisekoop, J. P. Monteiro, A. J. Yates, A. Y. Huang, and R. N. Germain, *Quantification of lymph node transit times reveals differences in antigen surveillance strategies of naive CD4+ and CD8+ T cells*, Proc Natl Acad Sci U S A, 109 (2012), pp. 18036–41.
[31] M. E. Meyer-Hermann and P. K. Maini, *Interpreting two-photon imaging data of lymphocyte motility*, Phys Rev E, 71 (2005), p. 061912.
[32] M. J. Miller, S. H. Wei, M. D. Cahalan, and I. Parker, *Autonomous T cell trafficking examined in vivo with intravital two-photon microscopy*, Proc Natl Acad Sci U S A, 100 (2003), pp. 2604–9.
[33] K. Murphy, *Janeway's ImmunoBiology*, Garland Science, New York, NY, 8th ed., 2011.
[34] S. P. Preston, S. L. Waters, O. E. Jensen, P. R. Heaton, and D. I. Pritchard, *T-cell motility in the early stages of the immune response modeled as a random walk amongst targets*, Phys Rev E, 74 (2006), p. 011910.
[35] S. Redner, *A guide to first passage processes*, Cambridge University Press, 2001.
[36] J. Reingruber and D. Holcman, *The narrow escape problem in a flat cylindrical microdomain with application to diffusion in the synaptic cleft*, SIAM Multiscale Model Simul, 9 (2011), pp. 793–816.
[37] H. Risken, *The Fokker-Planck equation. Methods of solution and applications*, Springer-Verlag, second ed., 1989.
[38] J. F. Rupprecht, O. Benichou, D. S. Grebenkov, and R. Voituriez, *Kinetics of active surface-mediated diffusion in spherically symmetric domains*, J. Stat. Phys., 147 (2012), pp. 891–918.
[39] S. L. Sanos, J. Nowak, M. Fallet, and M. Bajenoff, *Stromal cell networks regulate thymocyte migration and dendritic cell behavior in the thymus*, J Immunol, 186 (2011), pp. 2835–41.
[40] Z. Schuss, *The narrow escape problem - a short review of recent results*, J. Sci. Computing, 53 (2012), pp. 194–210.
[41] A Singer, Z Schuss, and D Holcman, *Narrow escape and leakage of brownian particles*, Phys Rev E, 78 (2008), p. 051111.
[42] A. Singer, Z. Schuss, D. Holcman, and R. S. Eisenberg, *Narrow escape, Part I*, J. Stat. Phys., 122 (2006), pp. 437–463.
[43] W. R. Smythe, *Static and Dynamic Electricity*, McGraw-Hill, New York, 1950.
[44] G. Szegö, *Ueber einige extremalaufgaben der potential theorie*, Math. Z., 31 (1930), pp. 583–593.
[45] A. Taflia and D. Holcman, *Dwell time of a Brownian molecule in a microdomain with traps and a small hole on the boundary*, J. Chem. Phys., 126 (2007), p. 234107.
[46] J. Textor, S. E. Henrickson, J. N. Mandl, U. H. von Andrian, J. Westermann, R. J. de Boer, and J. Beltman,

Random migration and signal integration promote rapid and robust T cell recruitment, PLoS Computational Biology, 10 (2014), p. e1003752.

[47] J. Textor, A. Peixoto, S. E. Hendrickson, M. Sinn, U. H. von Andrian, and J. Westermann, *Defining the quantitative limits of intravital two-photon lymphocyte tracking*, Proc Natl Acad Sci U S A, 108 (2011), pp. 12401–6.

[48] J. Textor, M. Sinn, and R. J. de Boer, *Analytical results on the beauchemin model of lymphocyte migration*, BMC Bioinformatics, 14 (2013), p. S10.

[49] M. J. Ward and J. B. Keller, *Strong localized perturbations of eigenvalue problems*, SIAM J. Appl. Math., 53 (1993), pp. 770–798.

[50] S. H. Wei, I. Parker, M. J. Miller, and M. D. Cahalan, *A stochastic view of lymphocyte motility and trafficking within the lymph node*, Immunol Rev, 195 (2003), pp. 136–59.

[51] T. Worbs and R. Förster, *T cell migration dynamics within lymph nodes during steady state: an overview of extracellular and intracellular factors influencing the basal intranodal T cell motility*, Curr Top Microbiol Immunol, 334 (2009), pp. 71–105.